NASA/TM-1999-209716

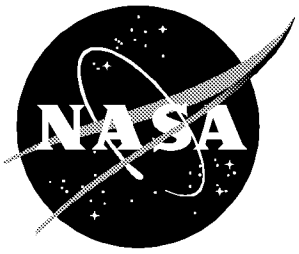

An Ozone Differential Absorption Lidar (DIAL) Receiver System for Use on Unpiloted Atmospheric Vehicles

Soenke Goldschmidt
Fachhochschule Ostfriesland
(University of Applied Sciences)
Emden, Germany

Russell J. DeYoung
Langley Research Center, Hampton, Virginia

November 1999

The NASA STI Program Office . . . in Profile

Since its founding, NASA has been dedicated to the advancement of aeronautics and space science. The NASA Scientific and Technical Information (STI) Program Office plays a key part in helping NASA maintain this important role.

The NASA STI Program Office is operated by Langley Research Center, the lead center for NASA's scientific and technical information. The NASA STI Program Office provides access to the NASA STI Database, the largest collection of aeronautical and space science STI in the world. The Program Office is also NASA's institutional mechanism for disseminating the results of its research and development activities. These results are published by NASA in the NASA STI Report Series, which includes the following report types:

- TECHNICAL PUBLICATION. Reports of completed research or a major significant phase of research that present the results of NASA programs and include extensive data or theoretical analysis. Includes compilations of significant scientific and technical data and information deemed to be of continuing reference value. NASA counterpart of peer-reviewed formal professional papers, but having less stringent limitations on manuscript length and extent of graphic presentations.

- TECHNICAL MEMORANDUM. Scientific and technical findings that are preliminary or of specialized interest, e.g., quick release reports, working papers, and bibliographies that contain minimal annotation. Does not contain extensive analysis.

- CONTRACTOR REPORT. Scientific and technical findings by NASA-sponsored contractors and grantees.

- CONFERENCE PUBLICATION. Collected papers from scientific and technical conferences, symposia, seminars, or other meetings sponsored or co-sponsored by NASA.

- SPECIAL PUBLICATION. Scientific, technical, or historical information from NASA programs, projects, and missions, often concerned with subjects having substantial public interest.

- TECHNICAL TRANSLATION. English-language translations of foreign scientific and technical material pertinent to NASA's mission.

Specialized services that complement the STI Program Office's diverse offerings include creating custom thesauri, building customized databases, organizing and publishing research results . . . even providing videos.

For more information about the NASA STI Program Office, see the following:

- Access the NASA STI Program Home Page at *http://www.sti.nasa.gov*

- Email your question via the Internet to help@sti.nasa.gov

- Fax your question to the NASA STI Help Desk at (301) 621-0134

- Telephone the NASA STI Help Desk at (301) 621-0390

- Write to:
  NASA STI Help Desk
  NASA Center for AeroSpace Information
  7121 Standard Drive
  Hanover, MD 21076-1320

NASA/TM-1999-209716

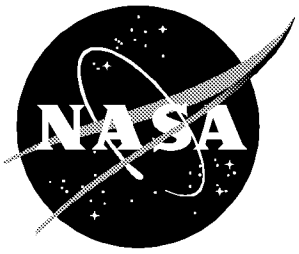

An Ozone Differential Absorption Lidar (DIAL) Receiver System for Use on Unpiloted Atmospheric Vehicles

Soenke Goldschmidt
Fachhochschule Ostfriesland
(University of Applied Sciences)
Emden, Germany

Russell J. DeYoung
Langley Research Center, Hampton, Virginia

National Aeronautics and
Space Administration

Langley Research Center
Hampton, Virginia 23681-2199

November 1999

Available from:

NASA Center for AeroSpace Information (CASI)
7121 Standard Drive
Hanover, MD 21076-1320
(301) 621-0390

National Technical Information Service (NTIS)
5285 Port Royal Road
Springfield, VA 22161-2171
(703) 605-6000

Contents

Abstract

Measurements of global atmosphere ozone concentrations call for flexible lidar systems that can be operated from an unpiloted atmospheric vehicle (UAV) to reduce the cost of measurement missions. A lidar receiver system consisting of a fiber-optic-coupled telescope has been designed and tested for this purpose. The system weight is 13 kg and its volume of 0.06 m^3 would fit into the payload compartment of a Perseus B UAV. The optical efficiency of the telescope is 37 percent at 288 nm and 64 percent at 300 nm. Atmospheric measurements with a DIAL laser system have been performed, and the measured ozone density has matched the data from ozonesondes to an altitude of 7 km.

1. Introduction

1.1. Importance of Atmospheric Ozone Measurements

Ozone is a very rare gas in our atmosphere, averaging about 3 molecules of ozone for every 10 million air molecules. But atmospheric ozone plays an important role that belies its small numbers. Most of the ozone is found within two regions of the Earth's atmosphere. Ninety percent resides in a layer between approximately 10 and 50 km above the Earth's surface, in the region of the atmosphere called the stratosphere, and is known as the "ozone layer." The remaining ozone is in the lower region of the atmosphere, the troposphere, which ranges from sea level up to about 10 km. The ozone molecules in the stratosphere and the troposphere both have the same chemical formula O_3, but depending on their location, they have very different effects on human and plant life.

Near the planet's surface or troposphere, ozone has direct contact with life forms and displays its destructive side. Because ozone reacts strongly with other molecules, high levels are toxic to living systems and can severely damage the tissues of plants and animals (ref. 1). Many studies have documented the harmful effects of ozone on crop production (ref. 2), forest growth (ref. 3), and human health (ref. 4).

In the troposphere, there is concern about increases in ozone. Low-lying ozone is a key component of smog, a familiar problem in the atmosphere of many cities around the world. Higher than usual amounts of surface-level ozone are now increasingly being observed in rural areas as well. To observe the changes of ozone in the troposphere, it is necessary to monitor its concentrations at different heights and global locations.

The substantial negative effects of tropospheric ozone contrast with the benefits of stratospheric ozone which filters ultraviolet-B (UV-B) radiation that would otherwise reach the Earth's surface and could cause skin cancer. Widespread scientific and public interest and concern about losses of stratospheric ozone exist. Ground-based, airborne, and satellite instruments have measured decreases in the amount of stratospheric ozone in our atmosphere. Over some parts of Antarctica, up to 60 percent of the total amount of ozone (known as the "column ozone") is depleted during September and October each year (ref. 5). This phenomenon has come to be known as the "ozone hole." Smaller, but still significant, stratospheric decreases have been seen at other, more populated regions of the Earth (ref. 5). Increases in surface UV-B radiation have been observed in association with decreases in stratospheric ozone.

The scientific evidence, collected over more than 2 decades of study by the international research community, has shown that human-made chemicals are responsible for the observed depletion of the ozone layer over Antarctica and likely play a major role in global stratospheric ozone losses (ref. 5). The ozone-depleting compounds contain various combinations of the chemical elements of chlorine, fluorine, bromine, carbon, and hydrogen and are often described by the general term "halocarbons." The compounds that contain only carbon, chlorine, and fluorine are called "chlorofluorocarbons," usually abbreviated as CFC's. CFC's, carbon tetrachloride, and methylchloroform are important human-made ozone-depleting gases that have been used in many applications including refrigeration, air conditioning, foam blowing, cleaning of electronics components, and as solvents. Another important group of human-made halocarbons is the "halons," which contain carbon, bromine, fluorine, and sometimes chlorine, mainly used in fire extinguishers. Governments have decided to discontinue productions of CFC's, halons, carbon tetrachloride, and methylchloroform, and industry has developed more "ozone-friendly" substitutes. The internationally agreed-upon Montreal Protocol and its Amendments call for elimination of the production and use of CFC's and other ozone-damaging compounds. As a result, the ozone layer is expected to recover over the next 50 years or so as the stratospheric concentrations of CFC's and other ozone-depleting compounds slowly decay.

Laser remote sensing from aircraft has become a very important technique for observing ozone in the environment. The Langley Research Center has an active aircraft-based research program which presently uses Nd: YAG-pumped dye lasers that are then doubled into the UV to probe both the stratosphere and troposphere for ozone with the differential absorption lidar (DIAL) technique (ref. 6). This large system can only fly on large (NASA DC-8 or the Electra) aircraft and has been deployed on many missions throughout the world (ref. 7). Airborne lidar applications have a great advantage in their flexibility of not being locally stationed. It provides the possibility to fly frequent missions over areas of interest and thereby monitor the changes of ozone during the seasons of the year at many diverse locations.

The acronym lidar stands for light detection and ranging, which is similar to radar but uses laser pulses instead of radio pulses. A pulsed laser beam is transmitted into the atmosphere. When the laser beam hits particles (either molecules or aerosols in the atmosphere) in its pathway some of the light is scattered back to a receiver system. The receiver system collects the backscattered light, processes it, and analyzes it. The measured data contain information about the height of the particles and the intensity of the scattering, which depends on the size of the objects and their number density.

Differential absorption lidar (DIAL) is a specialized lidar technique that not only detects the presence of molecules in the atmosphere but also can measure the absolute concentration as a function of altitude. These systems use two laser beams with different wavelengths called the "on-line" beam and the "off-line" beam. The wavelength of the on-line beam is turned to a higher absorption spectrum of the detectable molecule than the off-line wavelength, which has less absorption. Measuring the two different backscatter signal decays allows a calculation of the molecule density as a function of altitude.

1.2. Unpiloted Aircraft Vehicle Characteristics

In the future, it will be desirable to fly autonomous, lightweight, compact ozone DIAL instruments on unpiloted atmospheric vehicles (UAV). Such vehicles could fly at high altitudes for extended times collecting science data without risk to the operator. Cost for such missions may be substantially reduced over present large aircraft-based missions (ref. 7). Presently there are no ozone DIAL systems capable of flying on a UAV because of the high mass and power consumption of present ozone DIAL lidar systems. The characteristics of three UAV's are given in table 1.

1.3. Typical DIAL Ozone System Characteristics

In order to facilitate UAV missions, smaller more efficient laser transmitters need to be developed that emit approximately 20 mJ near 300 nm for each of the DIAL on- and off-line pulses. Also lightweight, compact DIAL receiver systems need to be built and demonstrated. Such receiver systems may incorporate fiber-optic-coupled telescopes for maximum light-gathering capability per unit area, high quantum efficiency gated photomultiplier tubes, and very narrowband filters for background light rejection with high light throughput. A compact high-performance digitizer and a data storage system are also required. A conceptional design of such an UAV DIAL instrument is shown in figure 1. The whole system is housed in the front payload compartment of the UAV, where windows in the hull allow optical transmission. A pulsed UV laser emits pulses into the atmosphere where elastic scattering and absorption occur. A small amount of this light is backscattered to the telescope by entering the compartment through a window. The received signal is converted into electrical pulses by the PMT followed by an amplifier and then digitized for further processing. An onboard computer system stores the received data.

A typical UAV payload compartment (fig. 1) has a length of less than 2 m, a volume of 0.7 m^3, and a maximum payload of 80 kg (ref. 8). These numbers show that the whole lidar system has to be compact and lightweight to fit into the UAV. The laser transmitter has to be lightweight and efficient and the weight and volume of the receiver system must be low. The system has to be robust and stable in optical, mechanical, and electronic adjustments to provide steady and accurate measurements during a radio-controlled flight.

1.4. Research Objectives

The objective of this investigation was the design, construction, and testing of a robust, compact ozone DIAL receiver system that could be a prototype for eventual use in a UAV ozone DIAL system. A second objective was to determine and minimize the size, weight, and power consumption of the whole receiver system as well as optimize its optical efficiency.

Table 1. General UAV Characteristics

Characteristic	Altus II	Perseus B	Pathfinder-Plus
Manufacturer of UAV	General Atomics/ Aeronautical Systems Inc.	Aurora Flight Sciences Corp.	AeroVironment, Inc.
Maximum payload, kg	150	80	45
Maximum payload power, kW	1.8 (single alternator) 2 to 5 (dual alternator)	1.0	0.5 to 1
Payload volume, m^3	0.733	0.7	NA
Maximum altitude, km	13.7 (single turbo) 20.0 (dual turbo)	20.0	24
Endurance, hr	24 at 10.7 km	18.6 at 20.0 km	6.5 at 18 km
Takeoff weight, kg	907	1100	330
Airspeed, m/s	33 to 36	41 to 150	27

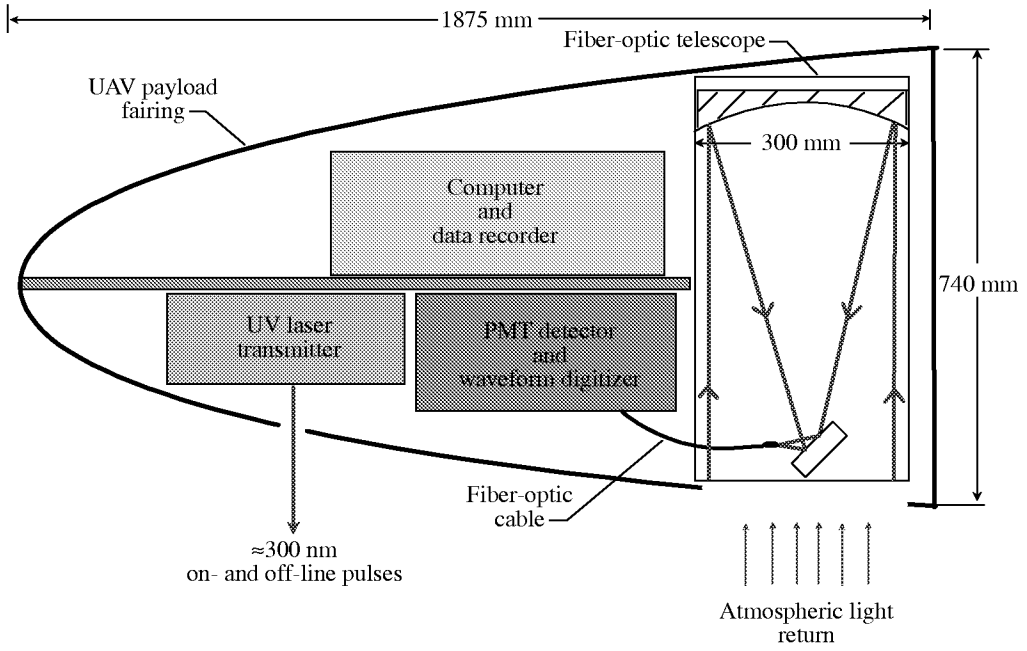

Figure 1. Side view of UAV payload compartment with typical ozone DIAL instrument.

An ozone DIAL receiver system was designed, constructed, and tested by using a fiber-optic-coupled telescope. The 30-cm-diameter mirror was attached to a carbon-fiber–epoxy tube to minimize mass. A lightweight PMT detector system was designed and built with a customized PMT gate circuit. The electronic signals from the PMT were processed by an advanced 16-bit digitizer and displayed and stored on a personal computer by using National Instruments LabVIEW software.

Measurements determined the optical efficiency of the telescope. Test measurements with the complete system were taken with a ground-based ozone DIAL system at a lidar laboratory at the Langley Research Center. A completely operational ozone DIAL receiver was constructed and used as a test bed for future UAV DIAL receivers.

2. Theory

2.1. Lidar Theory

2.1.1. Lidar Basics

The acronym “lidar” stands for light detection and ranging. The basic lidar setup is similar to the radar technique. The time between transmitting and receiving a signal is dependent on the distance from the object to the radar system. This distance can be calculated by knowing the speed of light and the fact that the signal has to travel from the source to the object and back. Instead of transmitting a radar pulse, the lidar system is operated with a laser transmitting a pulsed laser beam. The receiver system collects the backscattered light with a telescope usually positioned close to the laser system as shown in figure 2.

A photomultiplier tube (PMT) detector converts the received light signal into an electric pulse. This PMT uses the photoelectric effect to emit an electron from a photo cathode by hitting it with a photon. The signal can then be processed and analyzed by a digitizer and computer.

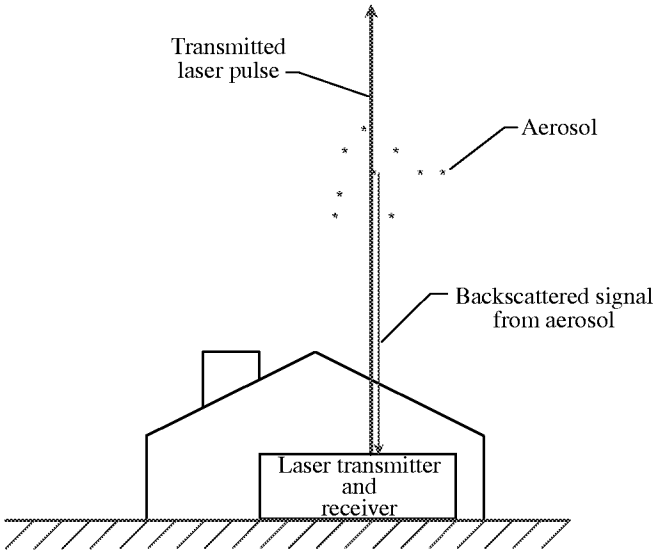

Figure 2. Ground-based lidar system.

2.1.2. Prediction of Atmospheric Return Signal

The received signal from atmospheric molecular elastic scattering can immediately be displayed on an oscilloscope for a rough visual analysis during the measurement. Accurate data analysis requires not only the digitizing of the data but also the compensation of optical losses in the atmosphere and the receiver system. In the atmosphere, the biggest loss is caused by the geometric probability that a molecule at a certain height scatters the signal back to the telescope. The expected lidar return signal can be predicted by the lidar equation.

2.1.3. Basic Lidar Equation

The basic lidar equation is shown in equation (1) (ref. 9). The equation relates the received optical energy E to the lidar system parameters. In this report only elastic backscattering is of interest for the measurements, and therefore the transmitted and received wavelengths are the same; thus,

$$E(\lambda, R) = E_L \, \xi(\lambda) \, T(\lambda, R) \, \xi(R) \, \frac{A_0}{R^2} \, \beta(\lambda, R) \, \frac{c\tau_d}{2} \tag{1}$$

where

$E(\lambda, R)$ scattered laser energy received by telescope just before PMT detector (λ is detected wavelength at receiver and R is range from detected molecule to receiver)

E_L output energy of transmitted laser pulse

$\xi(\lambda)$ receiver's spectral transmission factor including influence of any spectrally selecting elements like filters or mirrors

$T(\lambda, R)$ atmospheric transmission factor during transmission over range R

$\xi(R)$ probability of radiation at range R reaching receiver based on geometrical considerations

$\frac{A_0}{R^2}$ acceptance solid angle of receiver optics (A_0 is area of receiver mirror, R is range from scattering molecule to receiver)

$\beta(\lambda, R)$ volume backscattering coefficient

$\frac{c\tau_d}{2}$ detected pulse length, where τ_d is half-width of pulse, factor $1/2$ takes into account that transmitted signal has to travel $2R$ from transmitter to molecule and back to receiver, and c is speed of light.

This calculation can be used for single beam lidar systems like aerosol lidars.

2.1.4. DIAL Equation

The DIAL technique is used not only to detect the presence of particles in the atmosphere but also to determine the absolute concentration of ozone or water vapor as a function of altitude. The system in this report uses two different laser beams for ozone detection: the on-line beam and the off-line beam. The wavelength of the on-line beam is turned to a higher ozone absorption spectrum than the off-line wavelength, which is less absorbed. Measuring the two different wavelength backscattered lidar signals allows a calculation of the particle density at different altitudes. The return signal of the online beam is significantly weaker due to the greater atmospheric absorption by ozone. With the basic lidar equation (eq. (1)), the received power of a pulse $P_{\text{pulse}} = \frac{E}{\tau_L}$ (τ_L is time of laser pulse) can be written as

$$P(\lambda,R) = P_{\text{pulse}}\, T^2(\lambda,R)\, \beta(\lambda,R)\, \frac{c\tau_L}{2}\, \xi(R)\, \xi(\lambda)\, \frac{A_0}{R^2} \tag{2}$$

The DIAL equation is the ratio of the received powers from the on-line beam and the off-line beam as follows:

$$\frac{P_{\text{on}}(\lambda_{\text{on}},R)}{P_{\text{off}}(\lambda_{\text{off}},R)} = \frac{(P_{\text{pulse}})_{\text{on}}\, \xi(\lambda_{\text{on}})\, \beta(\lambda_{\text{on}},R)\, T^2(\lambda_{\text{on}},R)}{(P_{\text{pulse}})_{\text{off}}\, \xi(\lambda_{\text{off}})\, \beta(\lambda_{\text{off}},R)\, T^2(\lambda_{\text{off}},R)} \tag{3}$$

We assume that ξ_{on} and ξ_{off} have the same spectral transmission; thus, they cancel each other. Then the atmospheric transmission term can be substituted with (ref. 10)

$$\frac{T^2(\lambda_{\text{on}},R)}{T^2(\lambda_{\text{off}},R)} = \exp\left\{-2 \int_0^R [\kappa(\lambda_{\text{on}},R) - \kappa(\lambda_{\text{off}},R)]\, dR\right\} \tag{4}$$

where $\kappa(\lambda_{\text{on, off}},R)$ are the total atmospheric attenuation coefficients for the on-line and the off-line beams. Substituting equation (4) into equation (3) gives

$$\frac{P_{on}(\lambda_{on},R)}{P_{off}(\lambda_{off},R)} = \frac{(P_{pulse})_{on}\ \beta(\lambda_{on},R)}{(P_{pulse})_{off}\ \beta(\lambda_{off},R)} \exp\left\{-2\int_0^R [\kappa(\lambda_{on},R) - \kappa(\lambda_{off},R)]\, dR\right\} \tag{5}$$

Because we are interested in the ozone number density, we separate the part of the attenuation coefficient by shifting $\frac{\beta(\lambda_{on},R)}{\beta(\lambda_{off},R)}$ to the left side and taking the natural logarithm of both sides as follows:

$$\ln\left[\frac{P(\lambda_{on},R)}{P(\lambda_{off},R)}\frac{(P_{pulse})_{on}\ \beta(\lambda_{on},R)}{(P_{pulse})_{off}\ \beta(\lambda_{off},R)}\right] = -2\int_0^R [\kappa(\lambda_{on},R) - \kappa(\lambda_{off},R)]\, dR \tag{6}$$

The total attenuation coefficient can be decomposed into two separate terms:

$$\kappa(\lambda, R) = \bar{\kappa}(\lambda, R) + N(R)\ \Delta\sigma^{A}(\lambda) \tag{7}$$

where $\bar{\kappa}(\lambda, R)$ is the attenuation coefficient of the ozone absorption, $N(R)$ is the ozone number density, and $\Delta\sigma^{A}(\lambda)$ is the differential absorption cross section which is the difference between the ozone absorption cross section of the on-line and the off-line beams. Inserting equation (7) into equation (6) and taking the derivative result in

$$\frac{d}{dR}\ln\left[\frac{P(\lambda_{on},R)}{P(\lambda_{off},R)}\frac{(P_{pulse})_{on}\ \beta(\lambda_{on},R)}{(P_{pulse})_{off}\ \beta(\lambda_{off},R)}\right] = -2\left\{\left[\bar{\kappa}(\lambda_{on},R) + N(R)\ \Delta\sigma^{A}(\lambda_{on})\right] - \left[\bar{\kappa}(\lambda_{off},R) + N(R)\ \Delta\sigma^{A}(\lambda_{off})\right]\right\} \tag{8}$$

Solving for the ozone number density $N(R)$ results in

$$N(R) = -\frac{1}{2[\sigma(\lambda_{on}) - \sigma(\lambda_{off})]}\frac{d}{dR}\ln\left[\frac{P(\lambda_{on},R)}{P(\lambda_{off},R)}\frac{(P_{pulse})_{on}\ \beta(\lambda_{on},R)}{(P_{pulse})_{off}\ \beta(\lambda_{off},R)}\right] - \frac{\bar{\kappa}(\lambda_{on},R) - \bar{\kappa}(\lambda_{off},R)}{[\sigma(\lambda_{on}) - \sigma(\lambda_{off})]} \tag{9}$$

In order to simplify the equation, the differential absorption cross section is introduced:

$$\Delta\sigma = \sigma(\lambda_{on}) - \sigma(\lambda_{off}) \tag{10}$$

The on-line and off-line wavelengths are close to each other; therefore, we can assume that the backscattering coefficient β and the attenuation coefficient κ are independent of wavelength to arrive at the following equation:

$$N(R) = -\frac{1}{2\ \Delta\sigma}\frac{d}{dR}\ln\left[\frac{P(\lambda_{on},R)(P_{pulse})_{on}}{P(\lambda_{off},R)(P_{pulse})_{off}}\right] \tag{11}$$

Assuming that dR is very small gives an approximation to get to the basic DIAL equation for a range cell $\Delta R = (R_2 - R_1)$ as

$$N(R) = \frac{1}{2\,\Delta\sigma\,\Delta R} \ln\left[\frac{P(\lambda_{off},R_2)\,P(\lambda_{on},R_1)}{P(\lambda_{off},R_1)\,P(\lambda_{on},R_2)}\right] \tag{12}$$

Equation (12) compares the decay of the on-line signal and off-line signal in a defined range cell (usually 600 or 1050 m) as shown in figure 3. This shows that the DIAL calculation is not affected by the pulse power P, as long as a return signal from both beams is received for every calculated altitude. The smaller the range cell the more accurate the DIAL calculation of ozone will be. The calculation is based on the slopes of the lidar returns within a range cell.

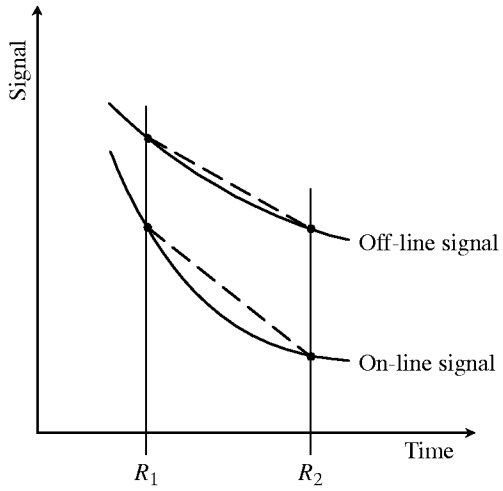

Figure 3. On- and off-line slopes within range cell $R_2 - R_1$ to determine ozone concentration within range cell.

2.2. Fiber-Optics Theory

2.2.1. Fiber-Optic Basics

Fiber-optic cables are used as optical transmission channels to guide light from one optical system to another. In the design of the telescope, a fiber-optic cable is used to couple the light from the telescope to the detector. It consists of a core (usually doped silica) with a high refractive index surrounded by a cladding (usually pure silica) with a slightly lower index of refraction as shown in figure 4. The advantage of using a fiber-optic cable to guide the light from the telescope to the detector is that it frees the user from the need for mirrors that have to be adjusted and cleaned.

The guidance of the light beam takes place by using the principle of total internal reflection to keep the light from leaving the core. Fiber-optic cables used in commercial applications have typically a core diameter of 5 to 50 μm, a cladding diameter of 125 μm, and losses of about 0.2 dB/km at 1550 nm. To protect the fiber from physical damage, a plastic or metal jacket usually covers the whole fiber. There are two different kinds of cables used today: single-mode fibers and multimode fibers. For the application in this investigation, only multimode fibers are used.

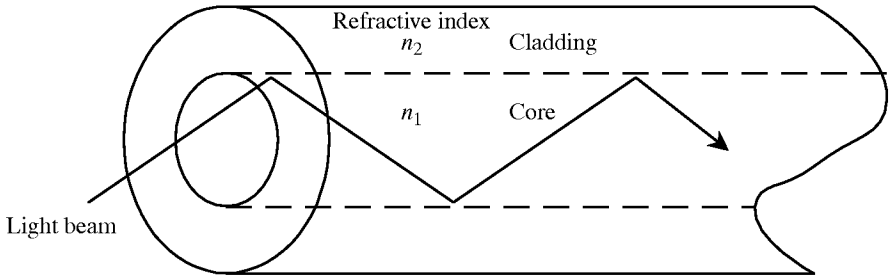

Figure 4. Typical optical fiber consisting of core and cladding.

2.2.2. Light Coupling With Fiber-Optic Cables

To couple a light beam into a fiber-optic cable, understanding the basic principles of optical reflection is necessary. If a light beam passes from a medium with refractive index n_1 to another with index n_2, the change of direction caused to the beam is formulated by Snell's Law (ref. 11) as

$$n_1 \sin \Theta_1 = n_2 \sin \Theta_2 \tag{13}$$

where Θ_1 is the angle of the incoming beam in medium 1 and Θ_2 is the angle of the outgoing beam in medium 2 as seen in figure 5. In this figure, medium 1 has a higher refractive index than medium 2 (i.e., from glass to air or from the fiber core to the cladding).

The light in a fiber-optic cable is conducted by total internal reflection at the contact surface between the core and the cladding. The core has a higher optical index n_1 than the index of the cladding n_2. With equation (13), it follows that Θ_2 is greater than Θ_1. For an angle of incidence $\Theta_1 = \Theta_c$, where Θ_c is called the critical angle,

$$n_1 \sin \Theta_c = n_2 \tag{14}$$

For this equation, the incoming light wave just grazes the contact surface of the core and the cladding and gets reflected back into the core as seen in figure 6.

2.2.3. The Numerical Aperture

Before a light beam can be coupled to the inside of a fiber-optic core, it has to enter the material of the core. The beam comes from an optical medium (usually air) with a low optical index to an optical medium with a higher index that is the fiber core. To couple the beam into the fiber core, the angle of entrance Ψ (fig. 7) is very important because it changes the internal reflection angle Θ. Equation (13) is used to get

$$\frac{\sin \Psi}{\sin \Theta} = \frac{n_1}{n_2} \tag{15}$$

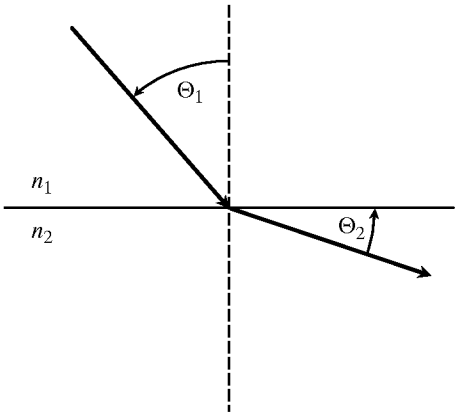

Figure 5. Transmission from high-index optical material to low-index material.

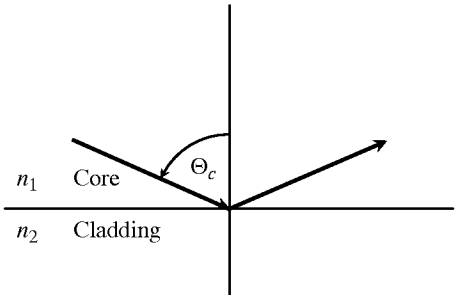

Figure 6. Total internal reflection in fiber-optic cable.

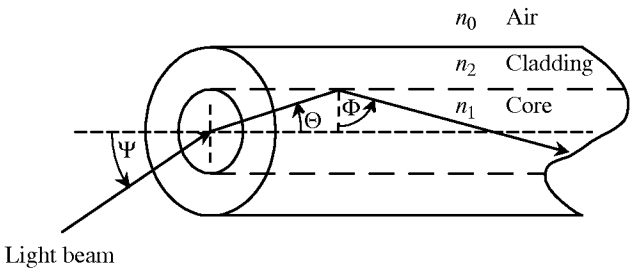

Figure 7. Light coupling into fiber-optic cable.

For total internal reflection it is necessary to have

$$\sin\Phi > \frac{n_2}{n_1} \tag{16}$$

After some transformation (ref. 11), we obtain

$$\sin\Psi_m = \sqrt{n_1^2 - n_2^2} \tag{17}$$

where Ψ_m is the maximum angle of entrance to achieve total internal reflection in the fiber core; this means that all light beams entering the fiber-optic cable at less than the angle Ψ_m will archive total internal reflection in the core. The term $\sin\Psi_m$ is also called the numerical aperture (NA) and is defined as

$$\mathrm{NA} = \sqrt{n_1^2 - n_2^2} \tag{18}$$

2.2.4. Fiber-Optic Beam Input Coupling

To couple the whole light beam into a fiber-optic cable, two conditions are necessary:

1. Focus the input beam in a way that all the light enters the fiber core at an angle that is smaller than the angle of entrance Ψ_m

2. Focus the input beam to the entrance of the fiber core such that the focal spot is smaller than the core diameter

Ideally the telescope focus would lead to an infinitely small focal diameter that would allow coupling into even the smallest fiber core. In the real world, we have to consider the effect of diffraction on the minimum focus diameter leading to a focal spot beam waist with a finite diameter. The diameter d_A of the so-called Airy disk containing 84 percent of the total energy from the Gaussian beam distribution is defined as (ref. 12)

$$d_A = 2.44\,\frac{\lambda f}{D} \tag{19}$$

where f is the focal length of the focusing mirror, λ is the wavelength of the beam, and D is the diameter of the focussing mirror. For example, the diffraction spot diameter for a telescope with a 30-cm diameter and a 60-cm focal length at 300 nm would be 1.5 μm, which is usually much less than the fiber-optic core diameter.

2.2.5. Fiber-Optics in Lidar Applications

Lidar receiver systems are similar to astronomical telescopes but their function is different. A standard astronomical telescope is an imaging system that collects the light from an object and focuses it in an eyepiece forming an image. A lidar receiver collects the backscattered light from a laser-illuminated spot from a finite distance and has no need for a sharp picture or image because the information of the

lidar return is contained in the intensity of the scattered light as a function of time. It is necessary to capture all the light backscattered from a minimum distance to infinity.

The numerical aperture of the fiber has to be compatible with the collecting telescope mirror *f*/*D* ratio, where *D* is the diameter of the collecting mirror, *f* is the focal length, and Ψ is the off-axis angle of the focused light as shown in figure 8. The relationship can be written as (ref. 13)

$$\frac{f}{D} = \frac{1}{2}\sqrt{\left(\frac{1}{\mathrm{NA}}\right)^2 - 1} \tag{20}$$

In figure 8 a smaller *f*/*D* ratio is seen to cause a larger angle of entrance Ψ leading to a larger NA to couple light into the fiber-optic cable. For a typical fiber-optic cable with an NA of 0.22, the telescope *f*/*D* ratio would be 2.2.

The light backscattering at different altitude causes the lidar return signal. If scattering occurs at high altitudes (i.e., 30 km), the received light can be assumed to be parallel when it reaches the telescope and the light gets focused from infinity to the telescope. Then the calculations for *f*/*D* can be calculated with equation (20).

For a backscatter signal from the near field (i.e., 1 to 3 km), the light reaching the telescope is not parallel and gets focused to a point deeper in the fiber-optic cable as seen in figure 9. To capture the whole lidar return, the fiber must be adjusted to the telescope such that it allows a coupling of the near-field signals as well as signals from the far field. The diameter of the fiber-optic cable has to be large enough to allow coupling of lidar signals even from the near field.

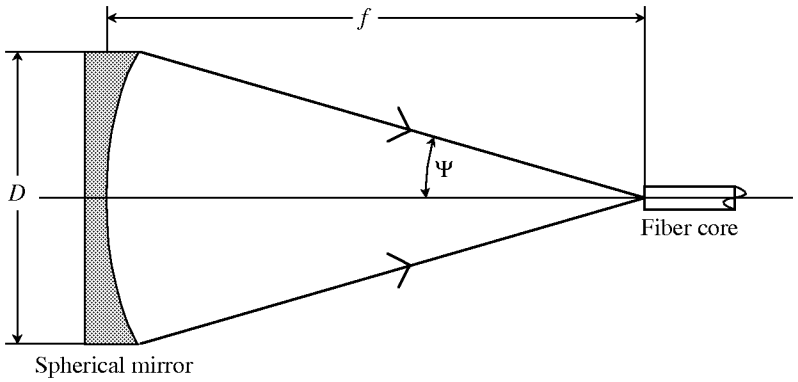

Figure 8. Ratio *f*/*D* of fiber-optic coupled telescope.

2.3. Photomultiplier Theory

A photomultiplier tube is an electro-optical device that converts light signals into electrical signals. A typical PMT setup with a data acquisition system for a fiber-optic-coupled PMT can be seen in figure 10. The optical components include a fiber-optic cable which guides the light to a collimating lens that enlarges the beam diameter and a narrowband filter to separate the wavelength of interest for the measurement. The PMT is connected to a high-voltage power supply that delivers the electric potential for the photocathode and the dynodes. To protect the PMT from saturation, a gate circuit is used to turn the PMT off during the near-field light signal for the first few microseconds after the laser has fired into the atmosphere. To process and store the measured data, the signal has to be amplified and digitized

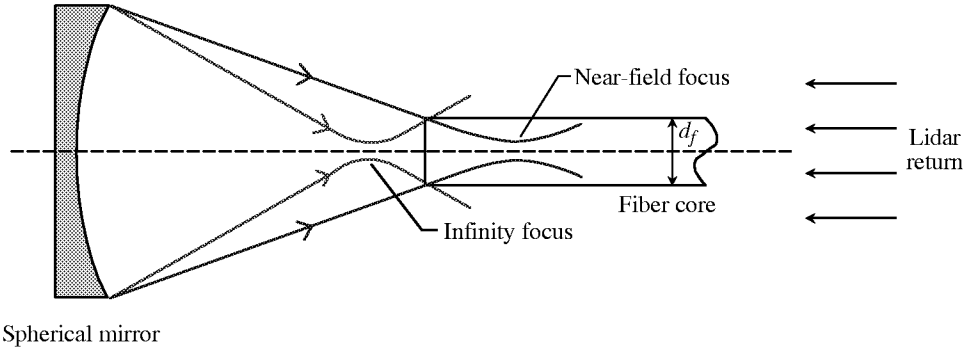

Figure 9. Near-field and far-field signal coupled into fiber-optic cable.

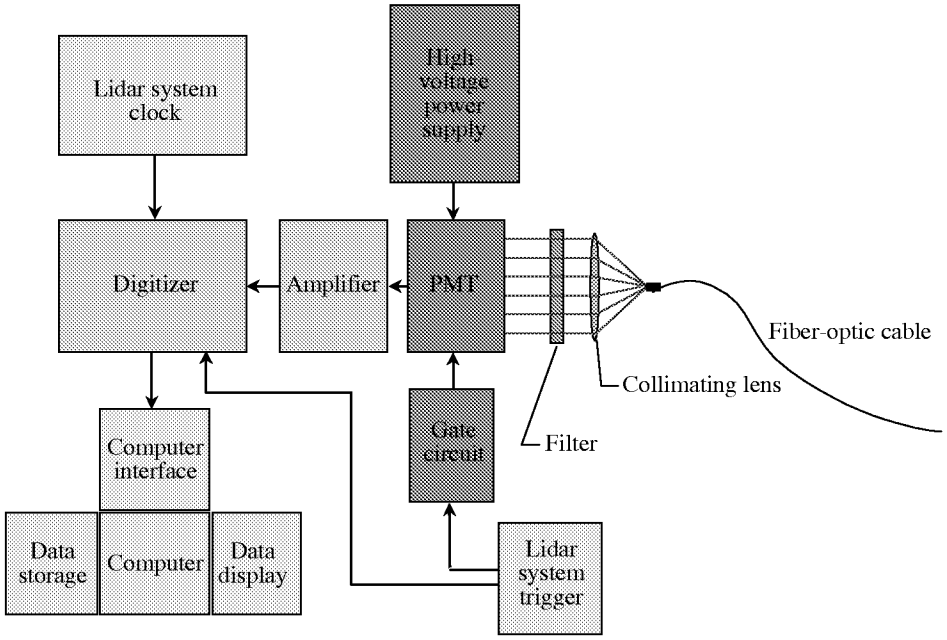

Figure 10. PMT setup for measurements with fiber-optic cable.

before entering the computer interface and the PC system where the process of analyzing, displaying, and storing is performed.

2.3.1. PMT Basics

A PMT consists of a photocathode and dynodes housed in an evacuated glass tube. When light enters the tube through a window, the photocathode emits an electron for nearly every incident photon. The dynodes are placed in the pathway of the emitted electron having an increasing positive electric potential. They create an electrostatic field that accelerates the electron and produces secondary electrons with every dynode stage. At the end of the dynode chain, an anode is placed to collect the electrons to form a current. This current is usually allowed to flow through a 50-Ω resistor creating a voltage signal. Figure 11 shows the basic setup of a PMT. The amplification of a PMT ranges from 10^3 to 10^8 and allows the detection of single photons (ref. 14). The material of the window of the tube has to be chosen for the detectable wavelength. The photoemissive material of the cathode is usually made out of a cesium compound like Cs-I, Cs-Te, or Sb-Cs. (See ref. 15.)

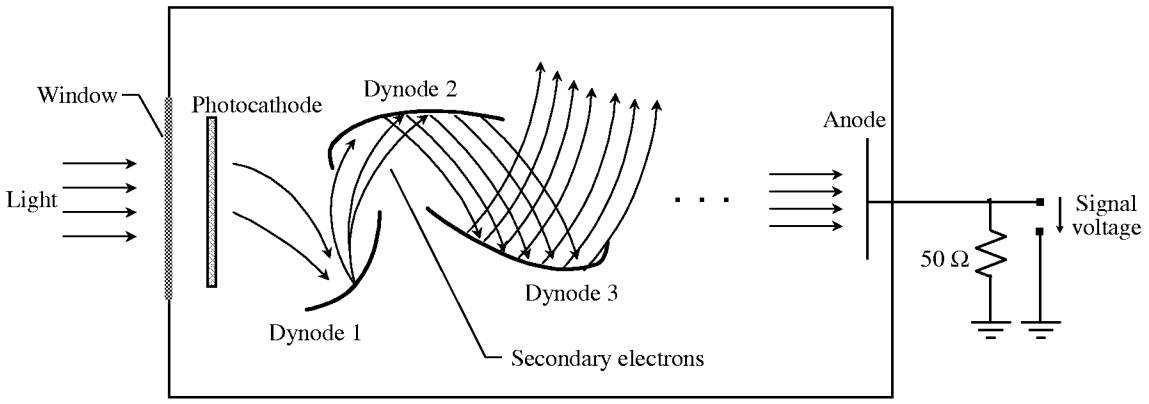

Figure 11. Basic setup of photomultiplier tube.

2.3.2. PMT Gain

The PMT gain depends on the number of dynode stages and the efficiency of the secondary emission caused by the single dynodes. Because the secondary electrons of one stage are the primary electrons of the next stage, the total gain μ is given by (ref. 14):

$$\mu = \delta n \tag{21}$$

where δ is the secondary emission coefficient per dynode stage (assumed to be equal for each stage) and n is the number of stages. In equation (21), all secondary electrons are assumed to be collected by the next dynode. Obviously either the larger number of dynodes or the design of very efficient dynodes leads to a higher gain. A high gain is useful to increase the signal to noise ratio. The gain also depends on the PMT voltage; a higher voltage between dynode stages accelerates electrons more and causes more secondary electrons to be admitted at the next dynode stage.

2.3.3. Gain Linearity and Saturation

The emission rate of the photoelectrons is proportional to the incoming light flux, and the number of secondary electrons for a given primary electron is proportional to the number of primary electrons. Therefore the anode current is proportional to the magnitude of the incoming light flux. A limit in this linear relationship occurs with the so-called space charge effect that is usually caused by the last three dynodes. The voltage gradient between the anode and the last dynode is generally much higher than between the other dynodes; this results in a limitation of multiplying at the previous stage (between the last two dynodes). By the use of an unbalanced dynode-voltage distribution, which increases the inter-stage voltages near the output end of the multiplier, increasing the linear range of the output anode current is possible. In this report, the adjustment is realized by using adjustable resistors on the last three dynodes to tune in the proper voltages.

The saturation phenomenon occurs at high light levels. The secondary electron collection efficiency of the anode degrades as the voltage between the last dynode and the anode decreases. Care must be taken to always operate lidar systems in their linear region.

2.3.4. Dark Current

The lower the intensity of the backscattered lidar return signal the lower is the signal to noise ratio. For very sensitive applications or weak laser sources, improving the signal to noise ratio is important. The largest source of noise is generally called the dark current, which can be caused by the following three major effects:

1. Ohmic leakage is a result of imperfect insulation of the glass stem, the supporting devices, or the base and is always present. This leakage is usually negligible but increases if water condenses on the tube or dirt builds up, which allows a higher leakage current. Ohmic leakage can be decreased by better insulation and keeping the tube dry and clean.

2. Thermionic emission is a current that is caused by the release of electrons from the photocathode or dynodes by thermionic emission. This emission occurs randomly in time and therefore the output dark current consists of random pulses. It also increases with the temperature of the PMT. Thermionic emission requires cooling of the whole PMT below room temperature.

3. Regenerative effects can be caused by several effects such as dynode glowing (dynodes start glowing under the bombardment with electrons), glass charging effects (emission of light from the inner glass surface), or afterpulsing (secondary pulses after detection of short laser pulses). Operating the PMT in its linear operation range can usually eliminate regenerative effects.

2.3.5. Quantum Efficiency

The photocathode quantum efficiency η is the ratio of the number of photoelectrons emitted by the photocathode divided by the number of incident photons and is generally expressed in percent. The photoemission takes place under a certain probability process. Photons with shorter wavelengths carry higher energy compared with those with longer wavelengths and result in an increase in the photoemission probability. For the detection of photons with short wavelengths in the region of 300 nm, PMT's are usually the best and most efficient detectors. PMT's that detect UV signals have higher quantum efficiencies than for visible signals.

3. Design of Receiver System

The design of the ozone DIAL prototype receiver is presented in this section. The discussion includes the mechanical design of the telescope, the design of the receiver optics, and the electronic design of the PMT gating and trigger circuits. This system was then tested with the existing laser system in the laboratory, and atmospheric measurements were performed.

3.1. Mechanical and Electronic Design of Telescope Receiver System

The design of the telescope hardware has to fulfill the lidar system requirements of low volume, lightweight, and energy efficient. Also, it has to be robust, easy to adjust, and give accurate measurements of atmospheric ozone.

3.1.1. Mechanical Design

The telescope consists of a spherical mirror housed in a carbon-fiber–epoxy tube, a turning mirror, and an adjustable mount for the fiber-optic cable. The telescope focuses the parallel light from the

back-scattered atmospheric return signal onto the turning mirror then into the fiber-optic cable. The other end of the fiber-optic cable is connected to a detector box, which contains a collimating lens, a narrowband filter, and the PMT detector. The receiver system in this investigation is used to detect ozone distributions in the atmosphere by using laser pulses in the UV-range of 300 nm. Therefore all the optical components (mirrors, lenses, filters, and the fiber-optic cable) have to have enhanced performance for this wavelength region. The design of the telescope focuses on two major topics: lightweight and accuracy under changing temperature conditions. The materials to achieve this were chosen to be carbon-fiber–epoxy for the main telescope tube and aluminum for the mirror mounting. Figure 12 shows the schematic setup of the ground-based telescope.

The carbon-fiber–epoxy tube is not only lightweight and stiff but also has a temperature expansion that is close to zero over the length of the tube because of the design of its carbon-fiber matrix. The zero expansion results in a constant distance between the spherical mirror and the mount for the turning mirror. The focal point does not change its position with temperature and this allows an optimum coupling of the beam into the fiber-optic cable.

3.1.2. Telescope Mirror and Tube

The telescope uses a spherical mirror with a clear aperture of 280 mm, a thickness of 50 mm, and a focal length of 610 mm. It has an aluminum coating with a magnesium fluoride overcoating for enhanced operation at 300 nm and has a mass of about 10 kg. The mirror is mounted in an aluminum ring that is glued onto the end of the tube. The carbon-fiber–epoxy tube is custom made with a matrix for zero expansion over the length during changes of temperatures. It has a diameter of 305 mm, a length of 610 mm, and a mass of about 1 kg.

3.1.3. Turning Mirror, Telescope Mounting, and Fiber-Optic Cable

The design of the telescope requires a mechanical connection between the telescope mirror and the turning mirror. The turning mirror has a diameter of 25 mm and a UV-enhanced coating. The center wavelength is 325 nm and its 45° reflectance is 99 percent. The mirror reflects the focused light at a right angle into the fiber-optic cable. The custom-made mounting for this mirror is positioned in the

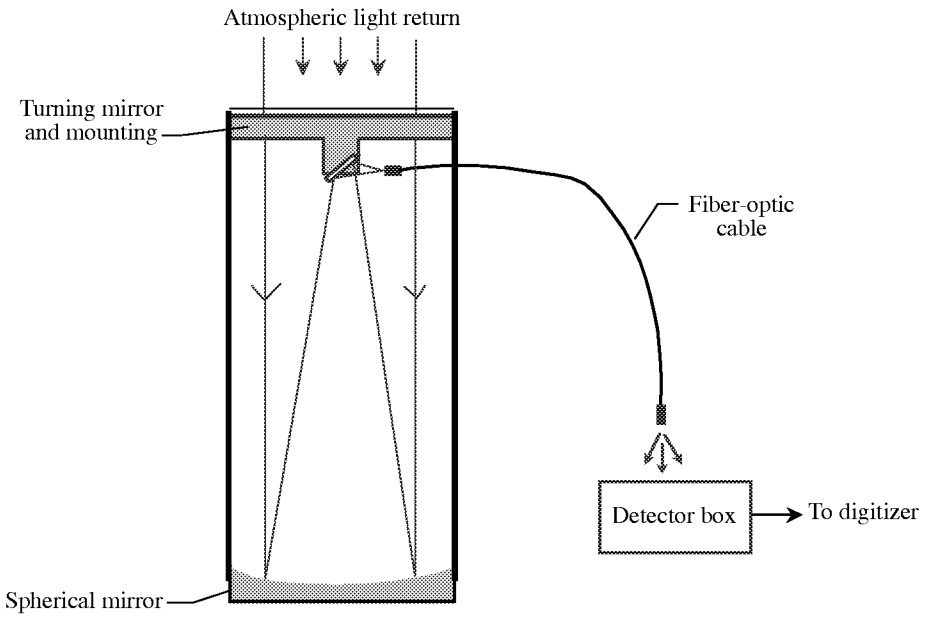

Figure 12. Fiber-optic-coupled telescope for lidar measurements.

pathway of the backscatterd lidar return signal and thus has to have a small profile for minimum blocking of the incoming light. Figure 13 shows the mounting for the turning mirror.

The mounting of the mirror is positioned inside the top of the carbon-fiber–epoxy tube and covers 3.5 percent of the clear aperture of the spherical mirror. The fiber-optic cable enters the tube through a hole beneath the mounting without covering any additional surface of the parabolic mirror. The end of the fiber-optic cable is attached to an adjustable "slider" that can be moved precisely by a screw to tune the optimum coupling length between spherical mirror and cable entrance.

A fiber-optic cable couples the focused beam from the telescope into the detector box. The fiber-optic cable is a UV1000/1100 T28 (NA = 0.28) step index fiber from CeramOptec, Inc. It has a core diameter of 1 mm, a length of 1 m, and a numeric aperture of 0.28. The core material is silica covered with doped silica cladding having a loss of 0.1 dB/m at 300 nm.

3.1.4. Detector Box Design

The light collected by the telescope is coupled into the fiber-optic cable and then sent to a detector box consisting of a collimating lens, a filter, and a PMT detector. The collimating lens has a 25-mm-diameter with a 50-mm focal length. It has an antireflection coating for reflecting less than 0.3 percent in the UV range of 300 nm. A narrowband filter with a transmission of 50 percent at 286 to 300 nm is used to block unwanted wavelengths from the detector. The photomultiplier tube used was a high quantum efficiency model Electron Tubes Photomultiplier Type 9125QSA. It is a 29-mm-diameter tube with 11 dynodes operated at −1100 V. The PMT delivers a maximum gain of 2×10^7 and has a quantum efficiency of 21 percent at 300 nm. The entrance window is made out of quartz and the photocathode is a bialkali type. All components are housed in a lighttight detector box for protection against background light; the detector box can be seen in figure 14.

3.1.5. Electronic PMT Gate and Trigger Circuit Design

The PMT gate circuit uses an electronic trigger signal to turn dynode 2, 4, and 6 of the PMT on and off, which allows the PMT to be operated only when a signal of interest is present. The PMT is turned off during the light return from the near field. The two circuits built in this system are the PMT gate

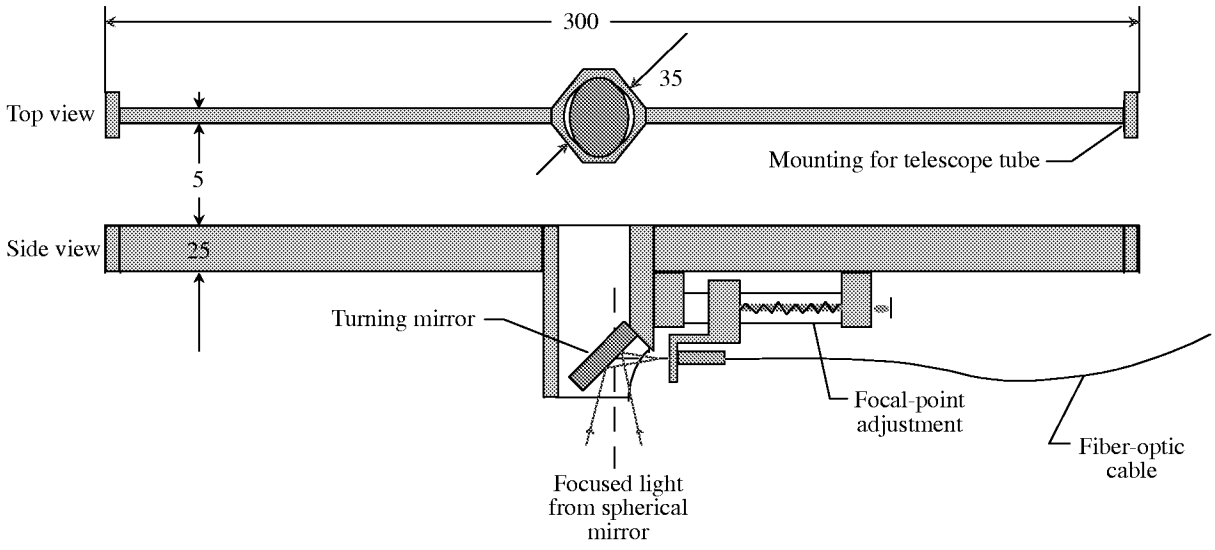

Figure 13. Turning mirror and its mounting. Dimensions are in millimeters.

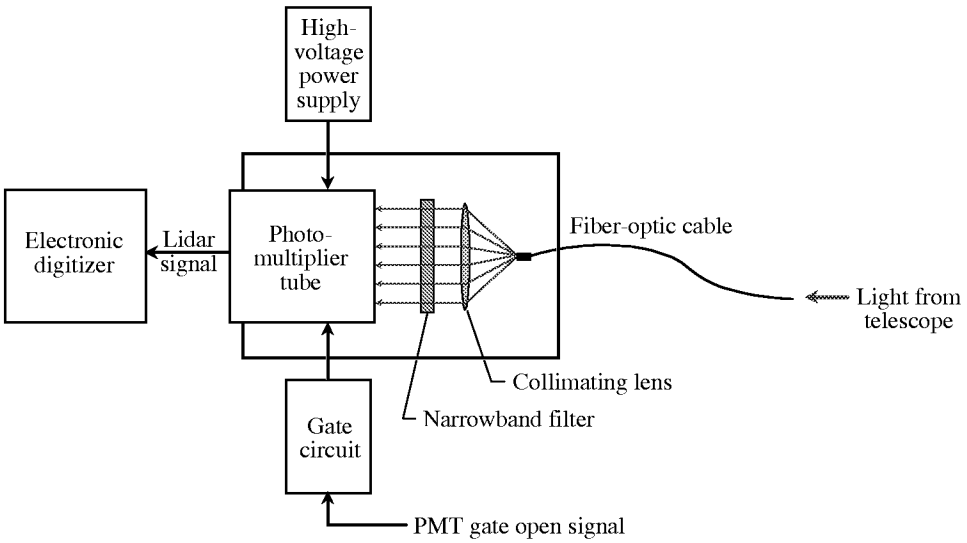

Figure 14. Detector box housing with filter and collimating lens and PMT detector.

circuit and an external trigger circuit that delivers a 90-V rectangle pulse for the triggering of the PMT gate circuit. Two separate 12-V batteries were used as a low noise power supply for the two circuits to separate the floating ground of the trigger circuit from the DC-DC converters for the high voltage.

The PMT circuit used can be seen in figure 15. The PMT gate circuit provides the PMT photocathode and dynodes with the necessary voltages between dynodes to accelerate the electrons towards the anode. The resistor chain works as a voltage divider to maintain the correct electric potential between the dynodes. The values of the dynode resistors R1, R2, and R3 are variable and have a great impact on the gain and linearity of the PMT. The two 0.047-μF and the 0.033-μF capacitors are used to couple the 90-V pulse applied to the PMT gate input to the dynodes 2, 4, and 6 to create the electric potential for the multiplying of the electrons when the PMT is turned on. The 0.1-, 0.2-, 0.3-, and 0.6-μF capacitors are used to keep the voltage high over the resistor chain when a high current is demanded due to the multiplying of the dynodes.

With no pulse applied to the PMT gate input, the voltage between the dynode pairs 1 and 2, 3 and 4, and 5 and 6 is the same for each pair. Therefore no electric potential builds up between the pairs and no electron multiplying occurs. When a 90-V pulse is applied to the PMT gate input, the voltages between these pairs are not the same anymore, and an electric potential builds up between each dynode pair. This build-up generates an increasing electric potential from dynode 1 to 6 towards the anode and allows the multiplying of electrons.

When light enters the tube through the PMT window, the photocathode emits an electron for every five incident photons. The electric field between the dynodes accelerates the electron and produces secondary electrons with every dynode stage. At the end of the dynode chain, the anode collects the electrons to form a current. This current flows through a 50-Ω resistor to create a voltage signal. The trigger signal of the gate is synchronized with the pulsed laser system having a delay of about 5 to 15 μs to eliminate the saturation caused by the near-field lidar return signal.

The gate trigger circuit shown in figure 16 was used to amplify a TTL rectangle pulse to a 90-V pulse that is capable of turning on the PMT gate circuit. The circuit uses its own battery because of a floating ground. The gate trigger circuit receives a TTL input signal ① from the master control of the

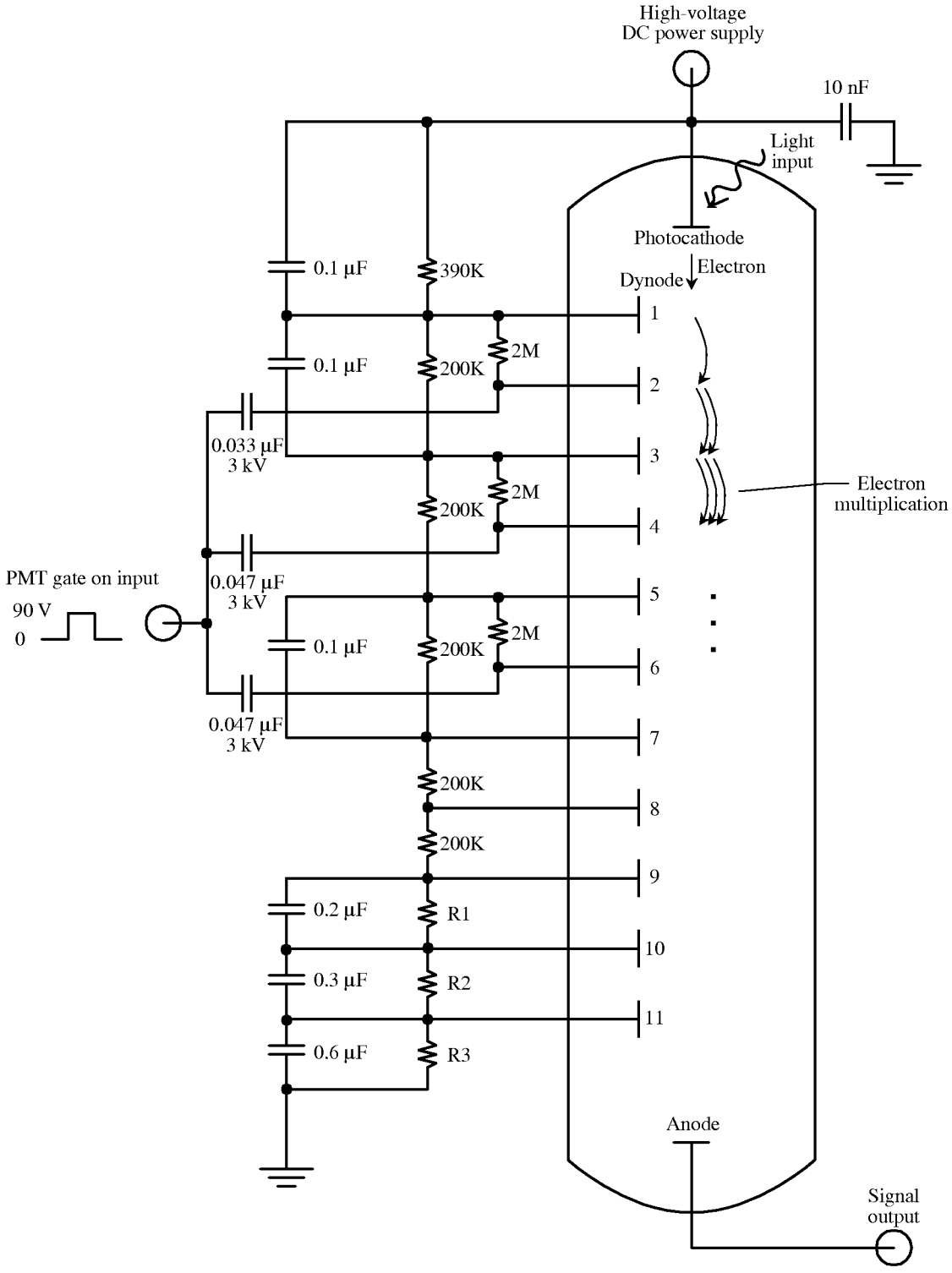

Figure 15. PMT gate and dynode chain circuit.

laser system, which is transformed into a light pulse by the optical transmitter ②. The light pulse is coupled through a fiber-optic cable to the optical receiver ③ that transforms it back into an electric signal, which is powered by the 5-V voltage regulator ④. The electrical isolation with the fiber-optic cable is done to separate the high-voltage part from the rest of the circuit with its floating ground. The driver

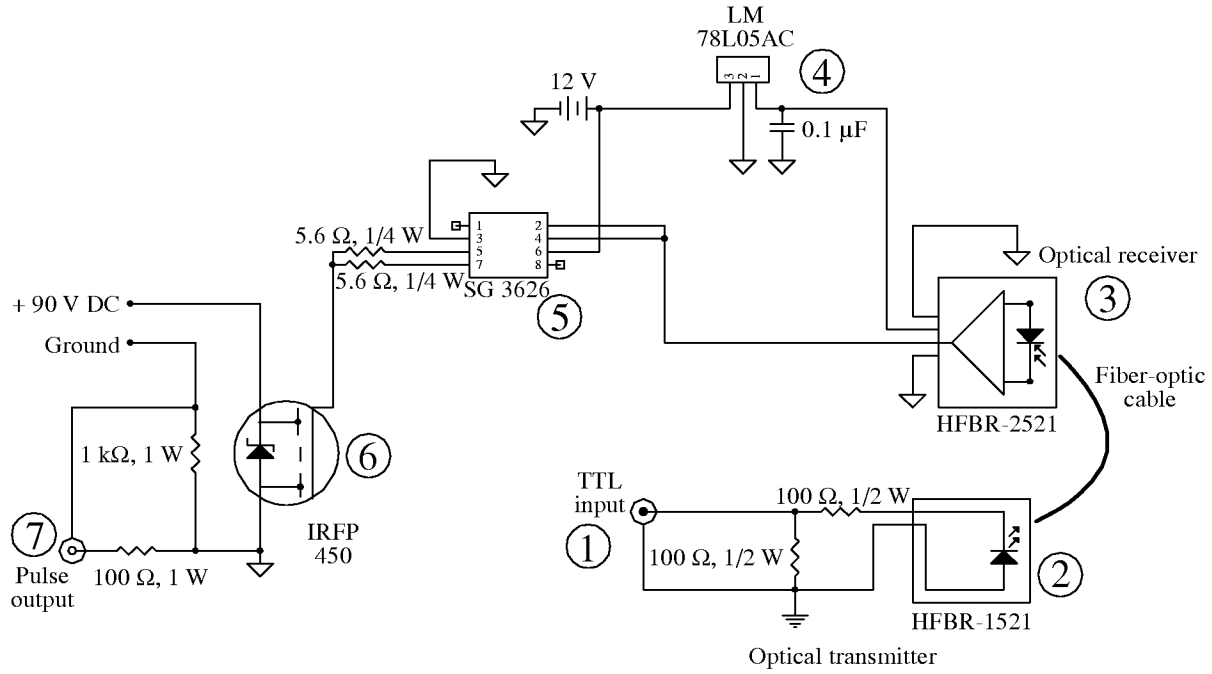

Figure 16. Gate trigger circuit schematic diagram.

⑤ for the power mosfet ⑥ inverts the electric signal from the receiver and amplifies its level to 12 V. The power mosfet is used to switch the 90 V across the 1-kΩ resistor forming a pulse output ⑦ to the gate input circuit of the PMT.

The high-voltage power supplies for the trigger circuit and the PMT are also housed in the circuit box. A DC-DC converter supplies the PMT circuit with −1100 V at a maximum current of 1.2 mA, and another DC-DC converter supplies the gating circuit with 90 V (10 mA maximum current). Both power supplies use a 12-V battery as a low noise power source.

4. Experimental Setup

The three experimental setups built during this investigation are discussed in this section. These are the setup used to adjust the PMT to the best linearity, the setup for measuring the optical efficiency of the telescope, and the setup to make ozone DIAL measurements with the ground-based laser system in the laboratory with the complete receiver.

4.1. Setup Adjustment of PMT Dynode Resistors

As stated in section 2, the voltage of the last three dynodes is very important for the PMT gain and its linearity for different light intensities. Variable resistors were used for the last three dynodes to adjust their values for maximum linearity of the PMT. For this purpose, the PMT was operated in a setup that allows monitoring the linearity with changing light intensities, and figure 17 shows the setup used.

The PMT was operated in a lighttight box by using a blue 470-nm light emitting diode (LED) as the light source and a 50-percent neutral density (ND) filter. The LED was connected to an adjustable power supply to vary the light intensity. The PMT was operated with the two power supplies (+90 V for the gate circuit and −1100 V for PMT resistor chain) by using a 12-V battery. The gate circuit was

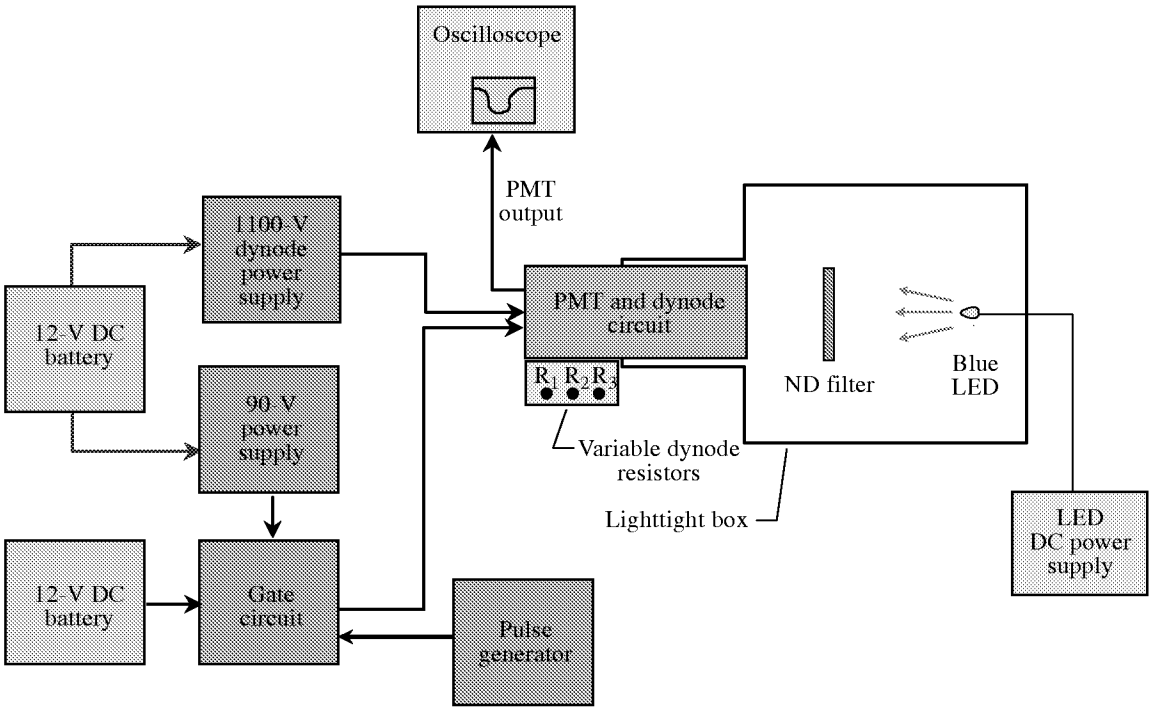

Figure 17. Setup for dynode resistor determination.

operated with a separate 12-V battery and supplied the PMT with a 90-V rectangle pulse that turned on the dynodes. A pulse generator supplied the gate circuit with a 5-V rectangle pulse that was used to trigger the 9 V. To measure the linearity output of the PMT, the PMT anode was connected to an oscilloscope with a 50-Ω load.

To determine the linearity of a certain resistor combination, the signal ratio was formed without a filter and with a 50-percent neutral density filter in front of the LED. These measurements were done by adjusting the dynode resistors to a certain value and then measuring the PMT output with an increasing light input without and with the ND filter. With perfect linearity, the ratio would be constant for all light intensities detected by the PMT. A systematic trial-and-error method was used to determine the optimum R1, R2, and R3 resistor values.

4.2. Telescope Optical Efficiency Setup

The optical efficiency of the telescope is measured by receiving a known amount of light with the telescope and measuring the light output at the end of the fiber-optic cable as seen in figure 18. The light source used for this measurement was a xenon continuous-wave (CW) lamp together with a monochromator for wavelength selection.

The light from the xenon lamp enters the adjustable monochromator which is dialed to a wavelength of 300 nm, and an additional filter was used to eliminate the multiple orders of the monochromator. The light is then coupled into a UV-enhanced fiber-optic cable that guides the light to the focal point of a large spherical laboratory mirror. This mirror has a standard aluminum coating with a reflectivity of 50 percent at 300 nm. The optical efficiency of the spherical laboratory mirror has been measured by Fredrik Lönn (ref. 16). The light output at the end of the fiber-optic cable was measured with a UV-enhanced silicon photodetector. The current of the detector was measured with a picoampere meter. The

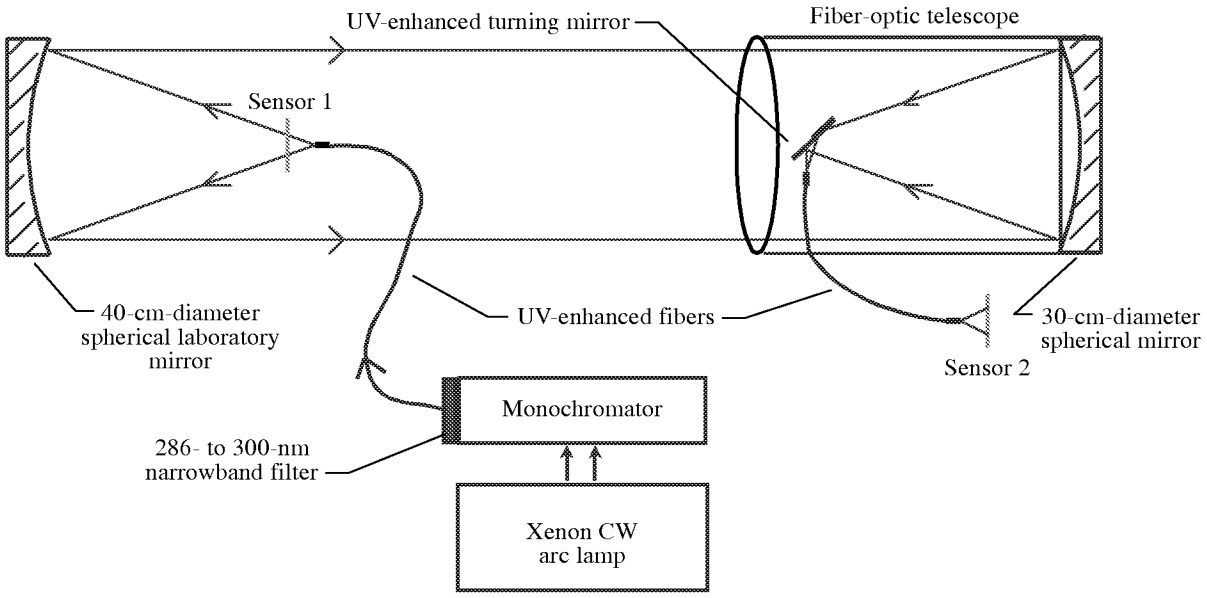

Figure 18. Setup for measurement of telescope efficiency.

detector was then removed and the light from the fiber-optic cable was collimated by the laboratory mirror and beamed towards the telescope. The telescope focused the parallel light onto the turning mirror and then into the fiber-optic cable as shown in figure 18. The turning mirror has a UV-enhanced coating for improved reflectivity at an angle of incidence of 45°. The optical efficiency can be calculated by forming the ratio of the light intensity entering the telescope $I_{\text{sensor2}}/R(\lambda)$ and the light intensity leaving the fiber-optic cable of the telescope I_{sensor1} as follows:

$$\eta(\lambda) = \frac{I_{\text{sensor1}}/R(\lambda)}{I_{\text{sensor1}}} \tag{22}$$

where $R(\lambda)$ is the laboratory mirror reflectivity as a function of wavelength from reference 16.

4.3. Ground-Based Ozone DIAL Measurement Setup

The testing of the system was accomplished by using a ground-based lidar setup operated with the existing laser system. The measurements taken during nighttime had very low background noise compared with those taken during daytime. The setup for these measurements can be seen in figure 19.

The laser system used for the ground-based ozone measurements was a doubled Nd:YAG laser-pumped dye laser. The output of the dye laser was doubled into the UV. Two separate lasers were operated at 288 nm for the on-line beam and 300 nm for the off-line beam. The energy of the pulses ranged from 15 to 20 mJ. The beam steering of the laser system was used to align the two laser beams vertically. The DIAL master controller delivers a pulse rate of 30 Hz to the laser and the PMT circuit as well as the 5-MHz time base for the digitizer. A hatch in the ceiling of the laboratory allowed the transmission of the laser beams as well as the receiving of the backscattered light to the telescope. The fiber-optic-coupled receiver was connected to the digitizer and PC system for the display and storage of the received data.

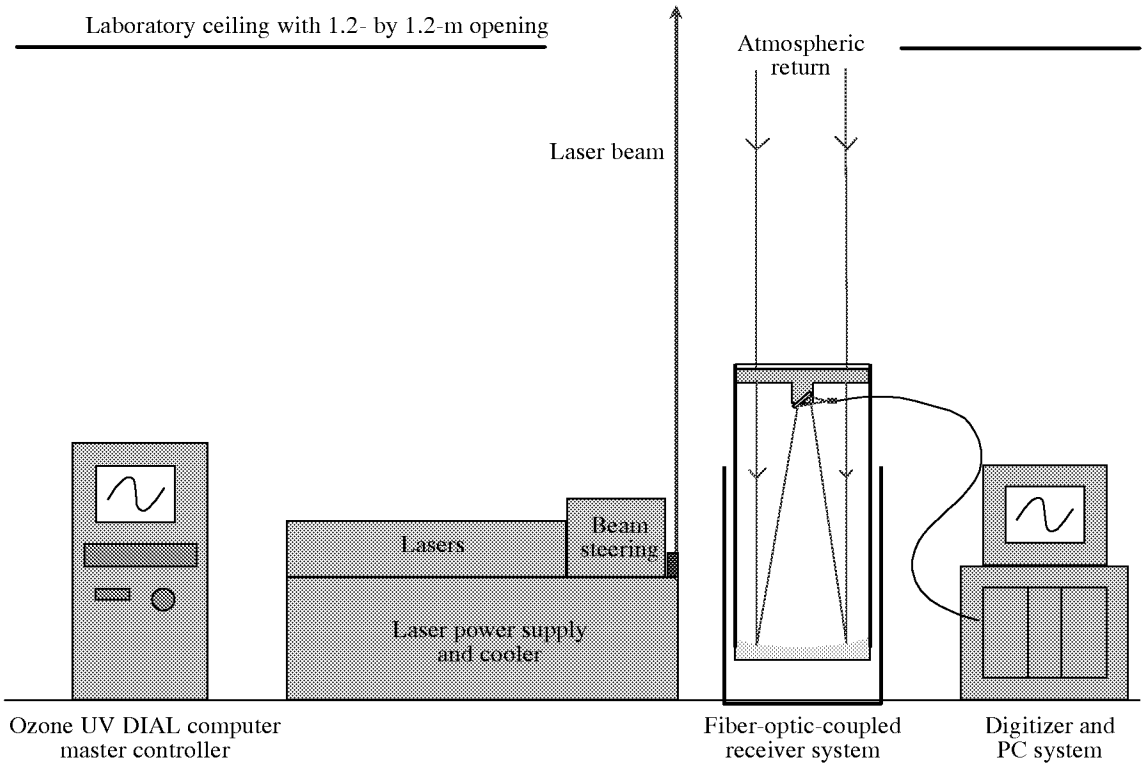

Figure 19. Ground-based ozone DIAL setup (not to scale).

The PMT used for this measurement was an Electron Tubes Photomultiplier Type 9125QSA operated at −1100 V. A 300-MHz amplifier was used to increase the anode signal by 10 times to improve the signal to the noise ratio sent to the input of the digitizer. Three 12-V batteries were used as power supplies for the detector system. One supplied the gate circuit, one was used for the high-voltage power supply, and one was used for the digitizer.

4.3.1. Telescope Alignment

Before performing a lidar measurement, aligning the telescope to the lidar return beam is necessary. For this purpose, the telescope is placed in a wider tube standing on two stepper motors and a pivot point for adjustment in the two vertical angles. The complete setup of the adjustable telescope can be seen in figure 20.

An aluminum ring in the middle of the carbon-fiber–epoxy tube is attached to two aluminum arms with a pivot point and two stepper motors to allow a mechanical connection to the outer tube and adjustments in the *X*-axis and *Y*-axis during measurements. A motion controller is used to operate two motors in single steps or continuous motion.

4.3.2. Data Acquisition System

The data acquisition system consisted of the digitizer and the computer system to store the detected data. The 16-bit digitizer was an Edge Technology ET2668-6 digitizer. The digitizer schematic can be seen in figure 21.

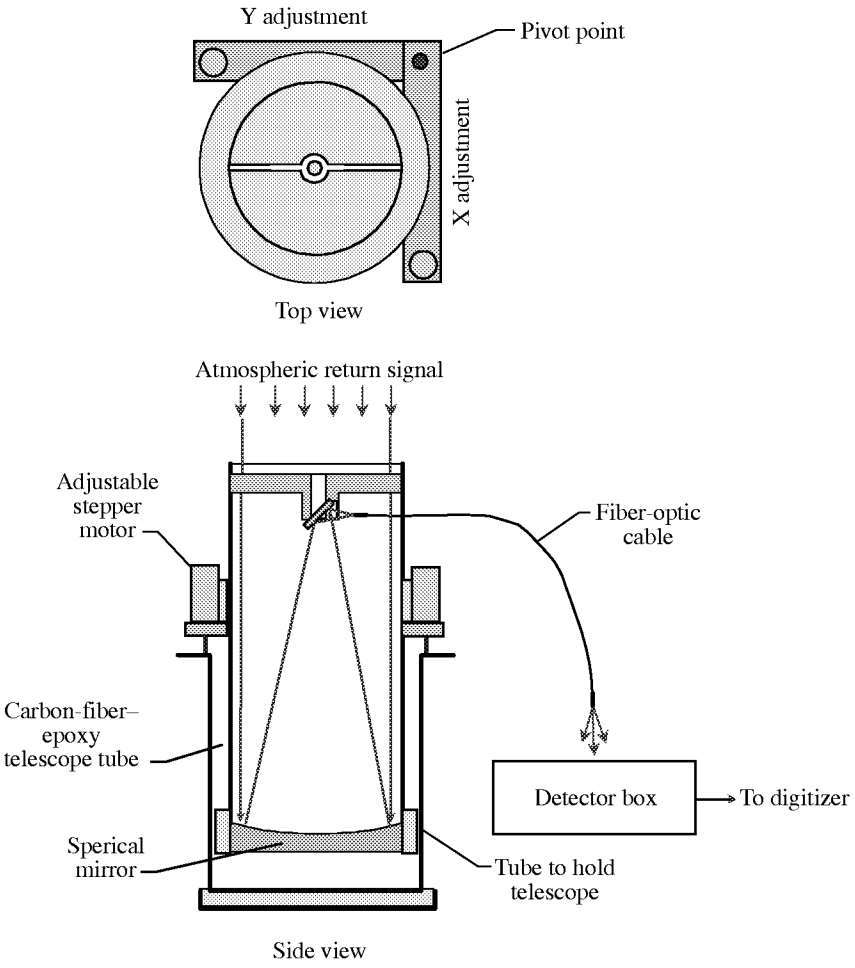

Figure 20. Adjustable fiber-optic-coupled telescope for ozone measurements.

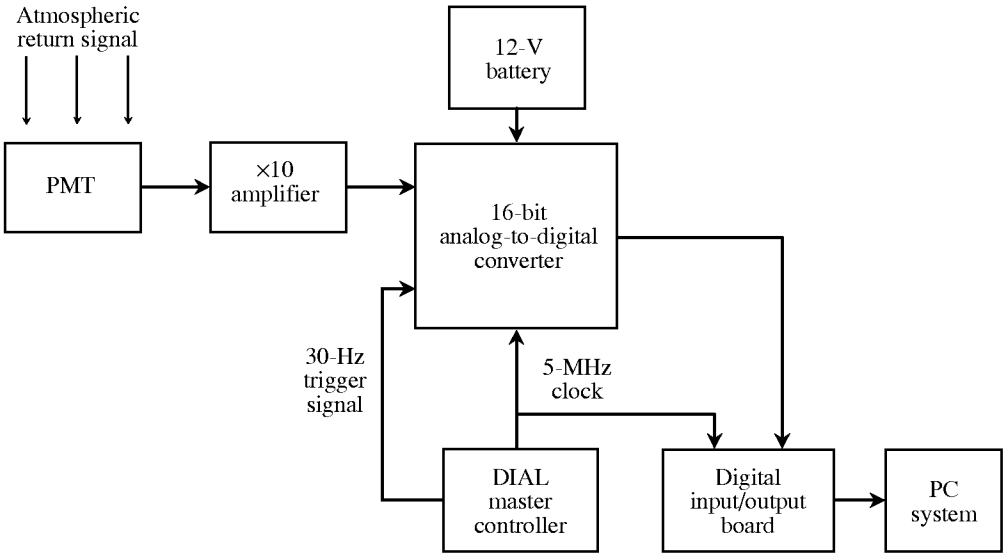

Figure 21. Data acquisition system.

In order to operate the digitizer it is necessary to supply a number of inputs: a 5-MHz time base to operate the digitizer, a trigger signal of 30 Hz to synchronize it with the laser pulses, and the amplified anode signal from the PMT. The 16-bit digitizer was operated at a clock rate of 5 MHz coming from the DIAL laser master control and has a ±1.5-V input voltage range. The output of the digitizer is connected to the digital input/output interface of the computer. The digitizer is operated in the range of 0 to −1.5 V due to the negative signal from the PMT and thereby delivers a resolution of 15 bits (32768 steps).

The computer system was a personal computer used to display, process, and store the signals from the digitizer through a digital input/output interface. The software used for this purpose was National Instruments LabVIEW software and allows an on-screen display of the raw data for a first visual view of the lidar return signal. After the measurement, the averaged return profile of 300 pulses was stored in a file for further processing.

5. Results and Discussion

5.1. Receiver System Mass, Volume, and Power Consumption

Because of the small volume and weight of the Perseus B UAV payload, the DIAL receiver prototype was designed for the limited aircraft specifications. For this purpose the components were chosen to be made from lightweight material and be compact.

The Perseus B is able to fly a mission with a maximum payload of 80 kg. The whole DIAL instrument has to fit into the front compartment of the UAV with most of the space and mass being used for the laser system. The mass of the DIAL receiver prototype is 16 kg, which includes the telescope (without its support frame), the detector box, and the electronics with batteries. The computer system and the DIAL master controller used for the ground measurements were not included. This weight uses 20 percent of the maximum payload mainly because of the high mass of the spherical telescope mirror (10 kg) and the batteries (3 kg).

The payload compartment of the Perseus B has a maximum volume of 0.7 m^3. The prototype DIAL receiver system uses a space of 0.057 m^3, which is mostly from the size of the telescope tube and represents a total use of 8 percent of the available volume.

The Perseus B payload power supply delivers 1 kW at 28 V DC, which is mainly needed for the laser system to achieve a high-energy laser beam. The power consumption of the PMT, the gate circuit, and the trigger circuit has a total consumption of 3.5 W and the digitizer 3 W, for a total receiver power consumption of 6.5 W, which represents a total payload power use of 0.7 percent.

5.2. PMT Dynode Resistor

As stated in section 3.1.5, the value of the last three dynode resistors of the PMT circuit are very important for the gain of the PMT. For this reason, variable resistors were used to determine the optimum values which were then replaced by resistors with fixed values. The setup for these measurements can be found in section 4. The PMT was operated at −1100 V for all measurements.

To determine the linearity of a certain resistor combination, a signal ratio was formed without a neutral density filter and with a 50-percent neutral density filter in front of the LED. These measurements were made by adjusting the dynode resistors to a certain value and then measuring the PMT output with an increasing light input without and with the filter.

The first step was adjusting all three resistors to be the same value. Figure 22 shows the results with different combinations and their impact on the PMT output at different light intensities.

The resistor combination of 140-140-140 kΩ showed the highest linearity. Therefore the next adjustment kept the first two resistor values at 140 kΩ and changed R3. Earlier test measurements showed that the last resistor needs a lower value than the previous one for maximum linearity. Therefore its value was lowered in steps as shown in figure 23.

The resistor combination of 140-140-100 kΩ showed the highest linearity. Next R1 and R3 were kept constant and R2 was changed. The results of this change are shown in figure 24. The resistor combination of 140-160-100 kΩ showed the highest linearity of all adjustments to a maximum anode current of 21 mA followed by a sharp drop in the linearity. This current is still smaller than the mean current of 33 mA stated by the manufacturer. This combination was kept as the final resistor adjustment for the last three resistors of the dynode chain.

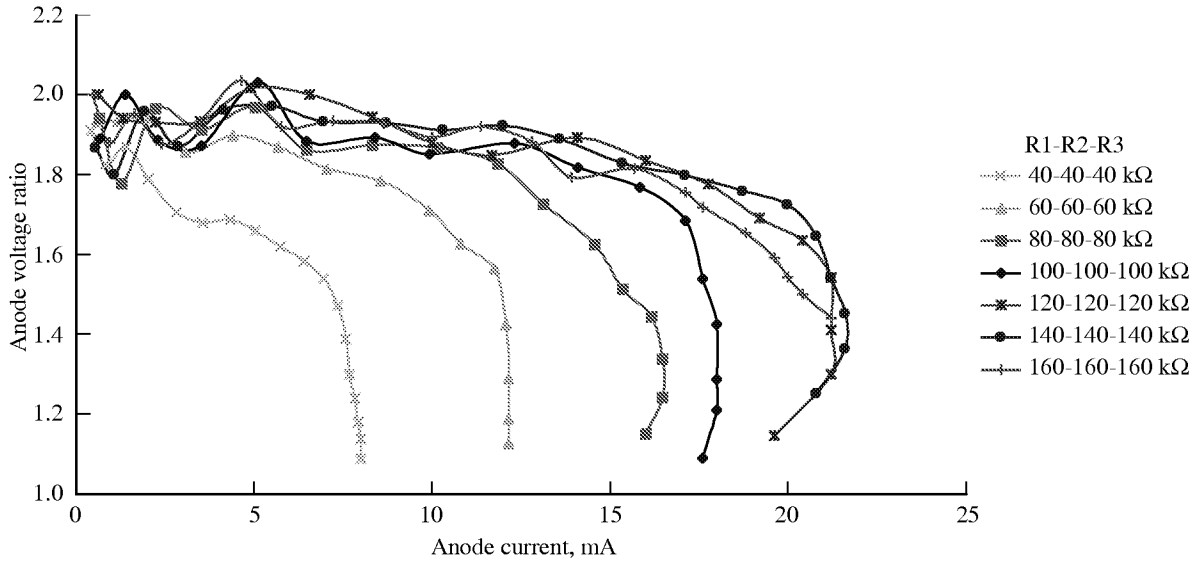

Figure 22. Adjustment of all three dynode resistors to same value.

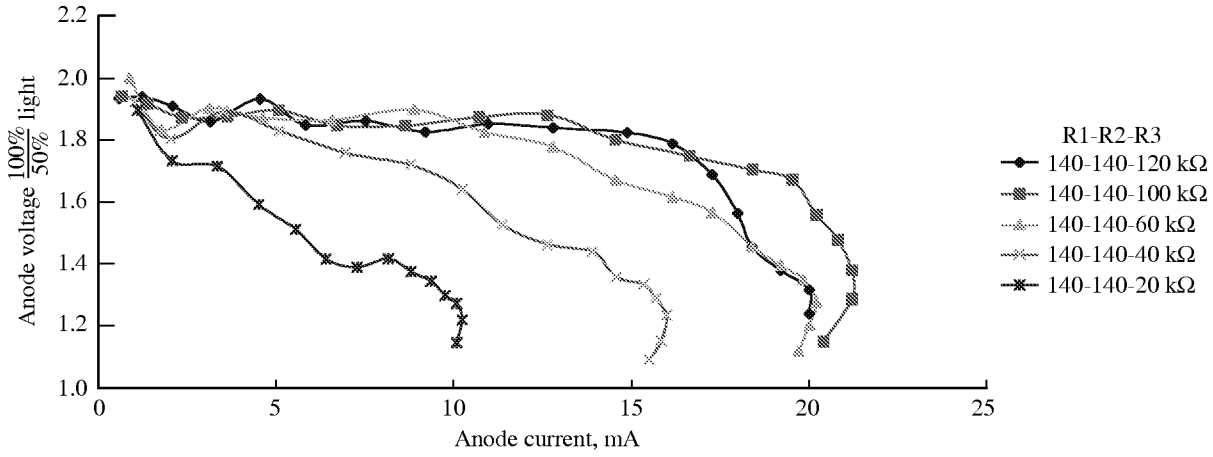

Figure 23. Adjustment of last dynode resistor R3.

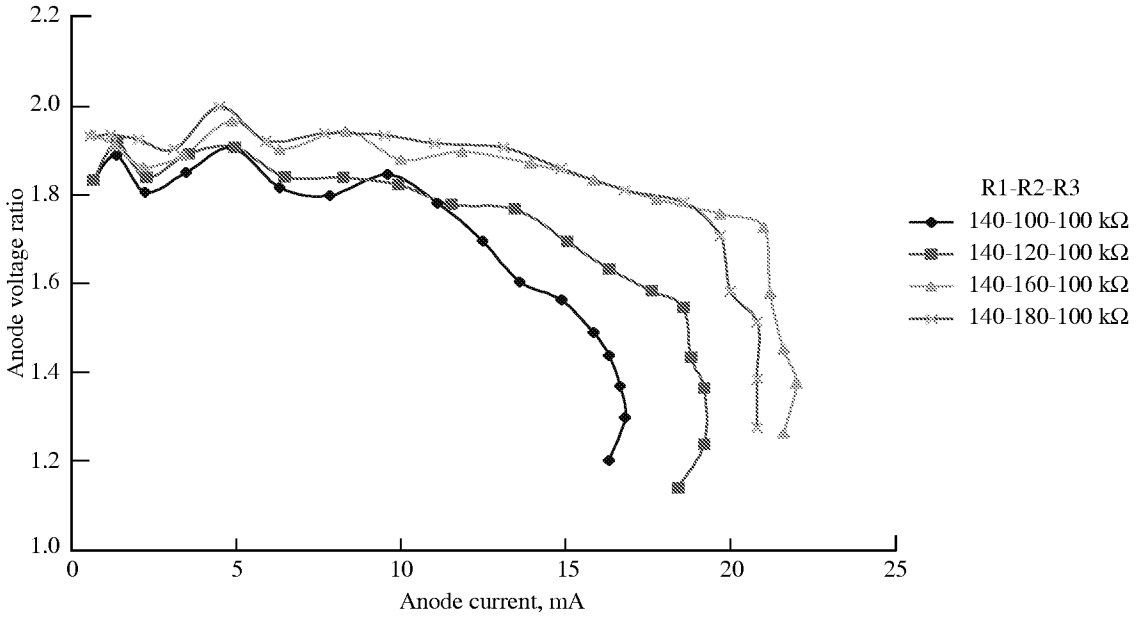

Figure 24. Adjustment of resistor R2 (dynode 10) with R1 and R3 constant.

5.3. Telescope Efficiency

The telescope efficiency determines optical light loss after entering the telescope and leaving it again through its fiber-optic cable. The efficiency was determined by forming the ratio of the amount of light entering the telescope (detector position 1) and the amount of light leaving the telescope (detector position 2). The setup for this measurement can be found in section 4. The result of this measurement can be seen in figure 25. Every displayed wavelength is an average of three measurements.

Figure 25 shows that the efficiency increases with the wavelength. The specifications from the manufacturers show a difference in loss of 1 percent for the spherical mirror and 0.3 percent for the fiber-optic cable between 288 and 300 nm. Thus, the loss of 27 percent between 288 and 300 nm comes mainly from the turning mirror used in the telescope. The wavelengths used for the ground-based DIAL measurement were 288 nm for the on-line beam and 300 nm for the off-line beam. The efficiencies for those two wavelengths are 37 and 64 percent.

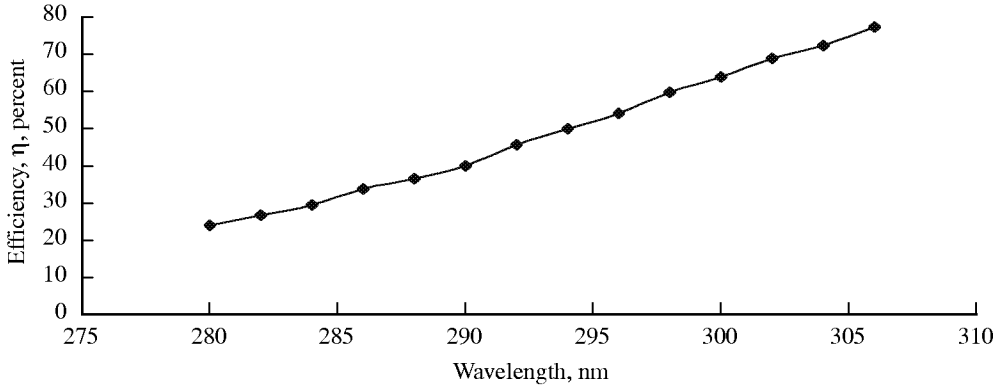

Figure 25. Optical efficiency of fiber-optic-coupled telescope as function of wavelength.

5.4. Receiver Ozone DIAL Measurement

This section shows the results of two ground-based DIAL measurements on January 4, 1999, and January 6, 1999, taken with the DIAL laser system at the Langley Research Center. These measurements are two examples of many measurements taken during this time. The setup for these measurements can be found in section 4. Figure 26 shows the raw data of a measurement from January 4, 1999, during the daytime and the exponential decay of the on-line beam and 300 μs later, the exponential decay of the off-line beam.

The digitizer value represents the lidar signal that ranges from 0 to 32767 (15 bits), which represents the amplified anode signal from 0 to −1.5 V. The X-axis gives the time elapsed after firing the laser. The PMT is gated on 5 μs after the laser fired the on-line beam to prevent the PMT from saturation from the near-field return signal. The time gate was on 275 μs, then the PMT is turned off for 5 μs during the firing of the off-line beam and turned on again for 275 μs after a delay of 5 μs.

A large peak can be seen at 30 μs (a height of 4500 m) for the on-line beam and at 330 μs for the off-line beam as a result of a cloud. This peak comes from the stronger backscattering of light caused by the water vapor in the cloud. The cloud did not absorb the entire laser beam; thus, a return signal from above the cloud was still received.

The DIAL measurement from January 6, 1999, was taken during a cloudless day with a gate delay of 13 μs and gives a good example of a raw signal return from a DIAL measurement. These data are shown in figure 27.

The return signals of the on- and off-line beams can be processed with the DIAL equation (eq. (12)) to obtain an ozone concentration profile. For this purpose, the signals from the on-line beam and the off-line beam have to be matched for every height. Subtracting the delay of 300 μs between the laser pulses from the return signal of the off-line beam results in an overlapping profile of both beams. This profile allows a direct comparison of the on-line beam and off-line beam as seen in figure 28. The raw data show a steeper decay for the on-line beam than for the off-line beam. This decay represents the stronger absorption of the on-line beam by ozone. Figure 28 also shows a steady signal after the laser signal had

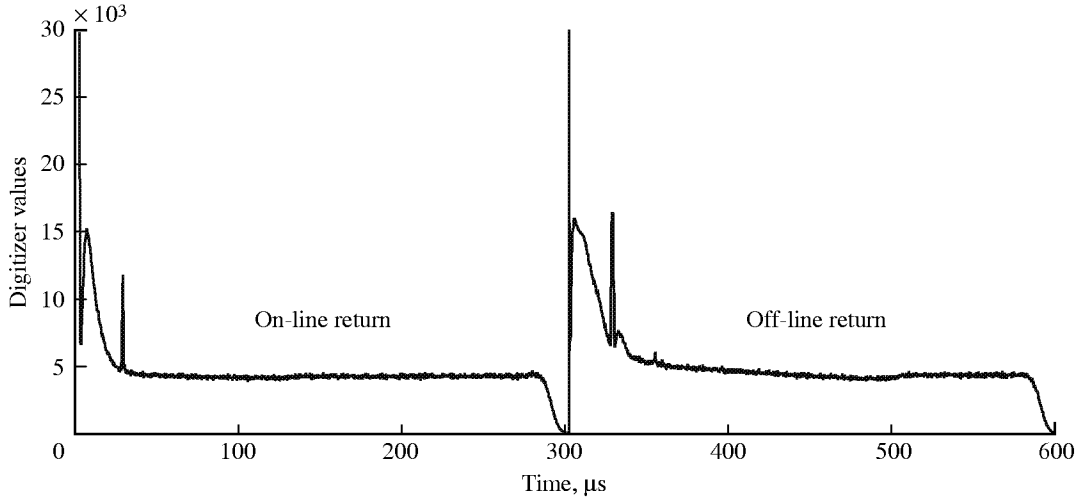

Figure 26. Raw DIAL data from January 4, 1999.

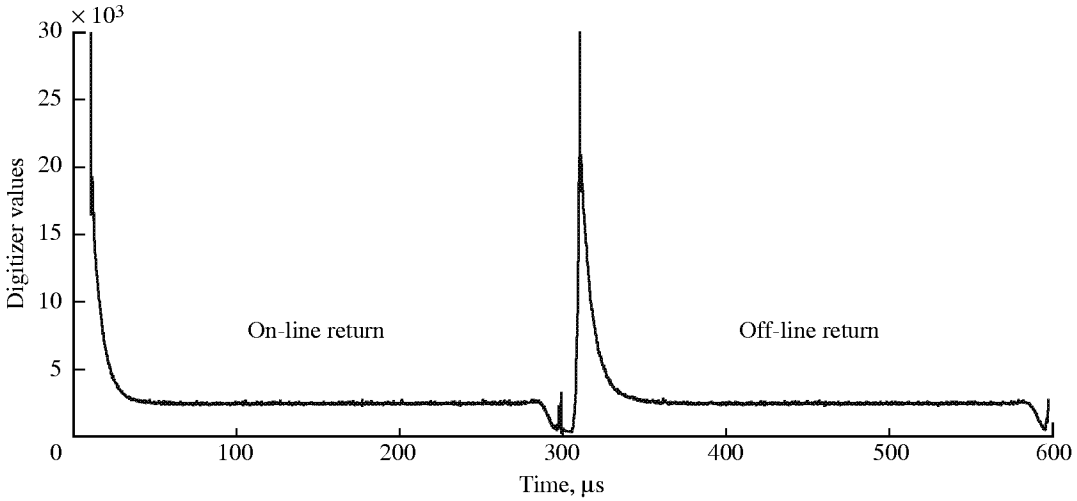

Figure 27. Raw DIAL data from January 6, 1999.

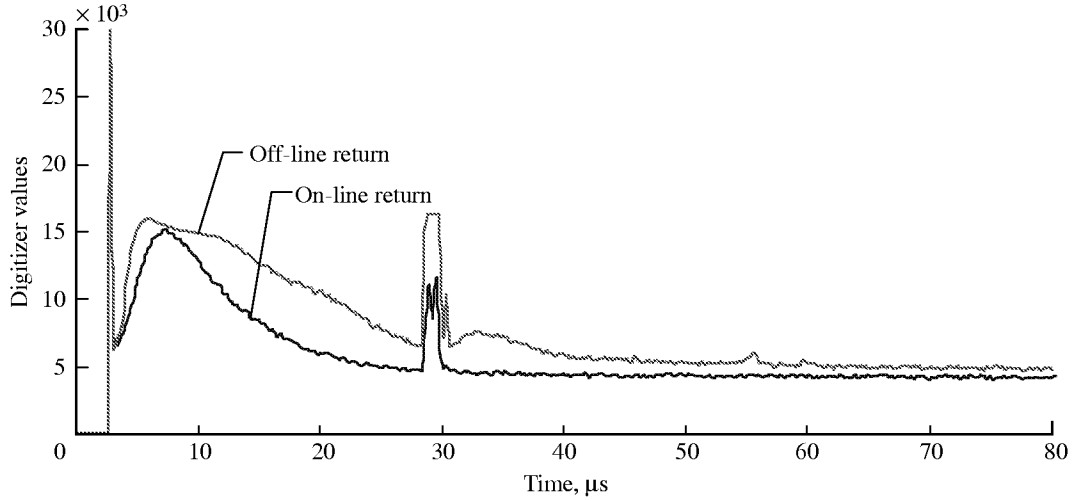

Figure 28. Height-corrected DIAL return signal from January 4, 1999.

been completely attenuated after a height of 80 μs (12 km). This signal is the background light level from the Sun that has to be subtracted for the DIAL calculation.

Figure 29 shows the results of the DIAL calculation from January 4, 1999. The three lines represent the DIAL calculations from 1.5 to 7 km with different range cells of 300, 600, and 1050 m. In figure 29 a smaller range cell results in a more accurate profile because of the finer steps taken in the DIAL calculation. A larger range cell results in a smoother profile that can average out errors caused by noise. The region above 4 km contains high noise because of the decreasing lidar signal returning from these heights. The range of 1.5 to 4 km shows an ozone profile with the concentration range usually found in this region with measurements from ozonesondes of about 1×10^{18} m^{-3}.

Figure 30 shows the best ozone profile taken with the DIAL receiver during this research effort. Depending on the range cell, the calculated profile contains high noise above 5.5 km for the range cell of 300 m and at 6.5 km for the range cell of 600 m.

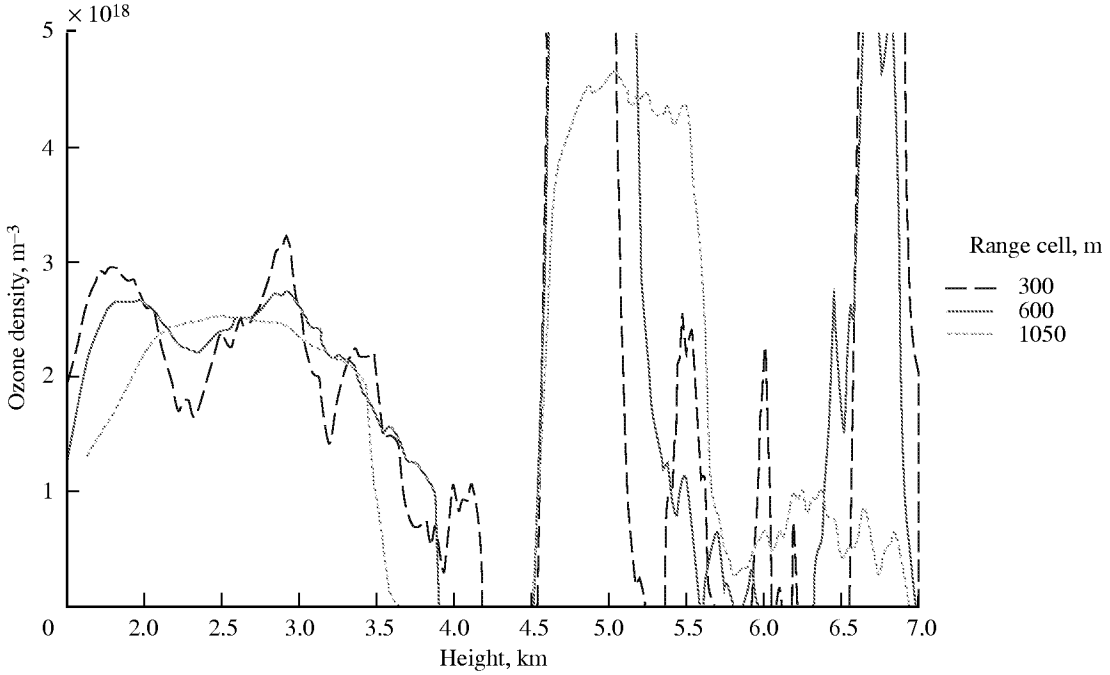

Figure 29. DIAL calculation of ozone concentration with different range cells from January 4, 1999.

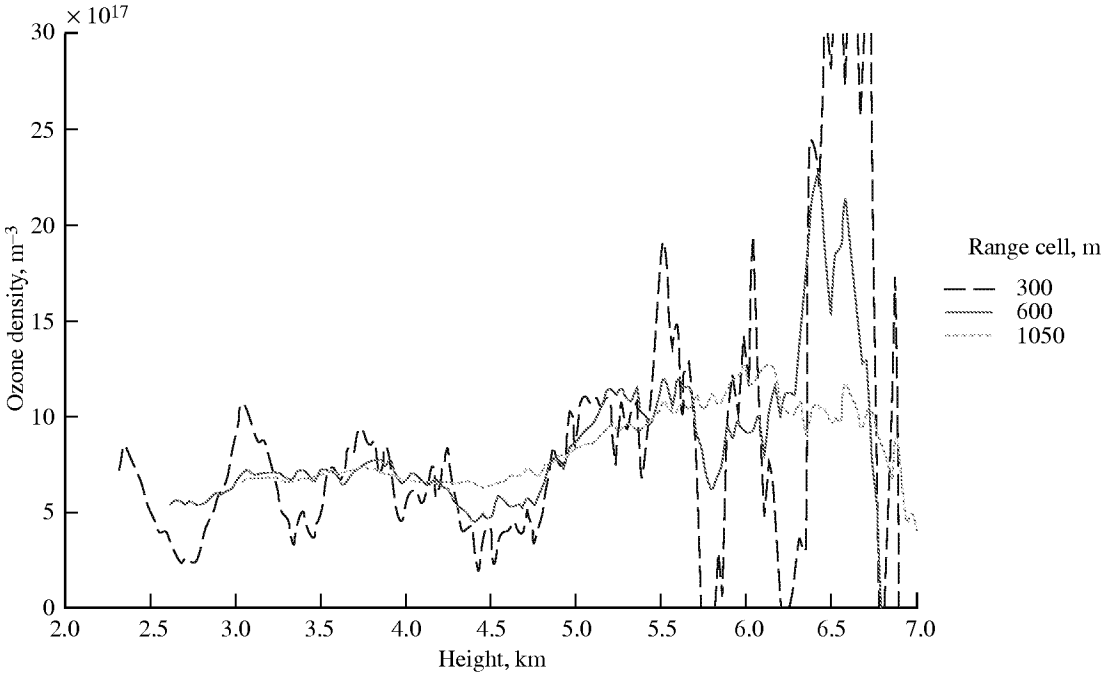

Figure 30. DIAL calculation of ozone concentration with different range cells from January 6, 1999.

5.5. Comparison of Data and Ozonesonde Measurements

The ozone DIAL measurement profiles were compared with the data from an ozonesonde. This ozonesonde (balloon sonde) uses an electrochemical cell to measure the ozone concentration in situ for

different heights. The ozonesonde was started on January 5, 1999, at the Wallops Flight Facility, which is 95-km northeast of the Langley Research Center. The ozonesonde is usually launched weekly on Wednesday mornings and therefore the data are only available for certain days. Because of the different times and geographic locations, the measurements differ somewhat in their profiles. Figure 31 shows the DIAL measurement from January 4, 1999, and the Wallops ozonesonde measurement from January 5, 1999. Figure 31 shows a higher variation between the two profiles in the region of 3 to 4.5 km because of the impact of local area ozone. At higher altitudes, a good match is seen because of the higher mixing ratios that give smoother ozone distributions over larger areas and is not as driven by local ground conditions.

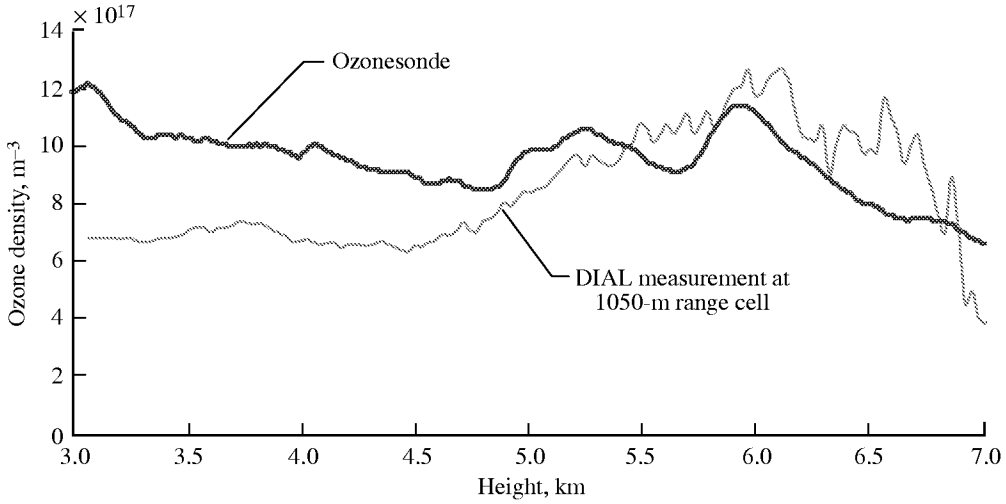

Figure 31. Measurements from DIAL taken January 4, 1999, and Wallops ozonesonde taken January 5, 1999.

6. Concluding Remarks

6.1. System Specifications

A complete ozone DIAL receiver system prototype for use on an unpiloted atmospheric vehicle (UAV) was designed, built, and tested and contained a fiber-optic telescope with a 300-mm spherical mirror and a 16-bit digitizer used for the data acquisition. The receiver system had a mass of 16 kg, a volume of 0.06 m^3, and a power consumption of 6.5 W and would fit in the payload compartment of a Perseus B UAV. The system was lightweight and rugged to fit the specification of the UAV payload compartment and the vibrations and temperature changes during a flight. The optical efficiency of the carbon-fiber–epoxy telescope was determined experimentally to be 37 percent at 288 nm and 64 percent at 300 nm including the losses caused by the telescopes spherical mirror, its turning mirror, and the fiber-optic cable. DIAL measurements were performed by using a Nd:YAG-pumped dye laser. Good agreement occurred between the DIAL ozone data and measurements taken with an ozonesonde from the Wallops Flight Facility. Because of the different locations and times the measurements were taken, the ozone profiles are reasonably close in magnitude.

An operational prototype ozone DIAL receiver system designed for operation from a UAV now exists at the Langley Research Center. This system could be used as a prototype for further development. It is small, lightweight, and has low power consumption and uses a carbon-fiber–epoxy

telescope tube, a fiber-optic cable for light coupling, and an advanced 16-bit digitizer for data acquisition.

6.2. Future System Improvements

During operation the telescope will face downwards in an airplane and will have to withstand the vibrations and movements during a flight. For this purpose, a fixed mounting will have to be designed that is independent from the orientation of the telescope. The alignment will be performed by adjusting the laser beam to the telescope. The power supplies used for the ground-based setup were three standard 12-V batteries for the trigger circuit, the PMT power supply, and the digitizer. These power supplies have to be minimized in their numbers and optimized in their weight. The PC system used for this investigation was a standard desktop one that can be replaced with a lightweight laptop or be included in the on-board computer system of the aircraft.

The design of the turning-mirror mounting included a hole over the turning mirror itself that was designed for future setups to allow an additional aerosol channel. The turning mirror would then not only reflect the return signal coming from the ultraviolet beam but would allow the passing of an additional beam for aerosols with a wavelength of 1 μm. This second channel would then be coupled into a second fiber-optic cable for processing in an additional detector system. For the optimization of the receiver weight the high mass of the spherical mirror used in the telescope could be reduced by using a mirror with a smaller mass, such as a carbon-fiber–epoxy mirror. To increase the range of the measurement, it is possible to use the photon-counting technique instead of the analog measurements performed in this investigation. This use would have a minimum impact on the present receiver design.

7. References

1. Adams, R. M.; Hamilton, S. A.; and McCarl, B. A.: An Assessment of the Economic Effects of Ozone on U. S. Agriculture. *J. Air Pollut. Control Assoc.*, vol. 35, 1985, pp. 938–943.

2. Heck, Walter W.; Cure, William W.; Rawlings, John O.; Zaragoza, Lawrence J.; Heagle, Allen S.; Heggestad, Howard E.; Kohut, Robert J.; Kress, Lance W.; and Temple, Patrick J.: Assessing Impacts of Ozone on Agricultural Crops—1: Overview. *J. Air Pollut. Control Assoc.*, vol. 34, no. 7, 1984, pp. 725–735.

3. Pye, John M.: Impact of Ozone on the Growth and Yield of Trees: A Review. *J. Environ. Qual.*, vol. 17, no. 3, 1988, pp. 347–360.

4. Lippmann, Morton: Health Effects of Ozone: A Critical Review. *J. Air Pollut. Control Assoc.*, vol. 39, no. 5, 1989, pp. 672–695.

5. *Scientific Assessment of Ozone Depletion, 1994*. NOAA, NASA, United Nations Environment Programme, and World Meteorol. Org., 1994.

6. Browell, Edward V.: Differential Absorption Lidar Sensing of Ozone. *IEEE Proc.*, vol. 77, 1989, pp. 419–432.

7. Browell, E. V.; Ismail, S.; and Grant, W. B.: Differential Absorption Lidar (DIAL) Measurements From Air and Space. *Appl. Phys. B: Lasers & Opt.*, vol. 67, 1998, pp. 399–410.

8. Aurora Flight Sciences Corp.: *Aurora Perseus B Unmanned Aerial Vehicle System Description*. Aurora Flight Sci. Corp., 1998.

9. Measures, Raymond M.: *Laser Remote Sensing: Fundamentals and Applications*. John Wiley & Sons, Inc., 1984.

10. Huffman, Robert E.: *Atmospheric Ultraviolet Remote Sensing*. Academic Press, 1992.

11. Ghatak, A. K.; and Thyagarajan, K.: *An Introduction to Fiber Optics*. Cambridge Univ. Press, 1998.

12. Smith, Warren J.: *Modern Optical Engineering: The Design of Optical Systems*, Second ed. McGraw-Hill Publ., 1990.

13. Jenness, James R., Jr.; Lysak, Daniel B., Jr.; and Philbrick, C. Russell: Design of Lidar Receiver With Fiber-Optic Output. *J. Appl. Opt.*, vol. 36, no.18, 1997, pp. 4278–4284.

14. Engstrom, Ralph W.: *Photomultiplier Handbook*. RCA Corp., 1980.

15. Hidehiro, Kume: *Photomultiplier Tube: Principle to Application*. Hamamatsu Photonics, 1994.

16. Lönn, Fredrik; and DeYoung, Russell: A Fiber-Optic Coupled Telescope for Water Vapor DIAL Receivers. *Nineteenth International Laser Radar Conference*, Upendra N. Singh, Syed Ismail, and Geary R. Schwemmer, eds., NASA/CP-1998-207671/PT2, 1998, pp. 857–860.

REPORT DOCUMENTATION PAGE

Form Approved
OMB No. 07704-0188

1. AGENCY USE ONLY *(Leave blank)*	2. REPORT DATE	3. REPORT TYPE AND DATES COVERED
	November 1999	Technical Memorandum

4. TITLE AND SUBTITLE
An Ozone Differential Absorption Lidar (DIAL) Receiver System for Use on Unpiloted Atmospheric Vehicles

5. FUNDING NUMBERS
WU 274-00-99-24

6. AUTHOR(S)
Soenke Goldschmidt and Russell J. DeYoung

7. PERFORMING ORGANIZATION NAME(S) AND ADDRESS(ES)
NASA Langley Research Center
Hampton, VA 23681-2199

8. PERFORMING ORGANIZATION REPORT NUMBER
L-17855

9. SPONSORING/MONITORING AGENCY NAME(S) AND ADDRESS(ES)
National Aeronautics and Space Administration
Washington, DC 20546-0001

10. SPONSORING/MONITORING AGENCY REPORT NUMBER
NASA/TM-1999-209716

11. SUPPLEMENTARY NOTES
Goldschmidt: Fachhochschule Ostfriesland (University of Applied Sciences), Emden, Germany; DeYoung: Langley Research Center, Hampton, VA.

12a. DISTRIBUTION/AVAILABILITY STATEMENT
Unclassified–Unlimited
Subject Category 74 Distribution: Standard
Availability: NASA CASI (301) 621-0390

12b. DISTRIBUTION CODE

13. ABSTRACT ***(Maximum 200 words)***

Measurements of global atmosphere ozone concentrations call for flexible lidar systems that can be operated from an unpiloted atmospheric vehicle (UAV) to reduce the cost of measurement missions. A lidar receiver system consisting of a fiber-optic-coupled telescope has been designed and tested for this purpose. The system weight is 13 kg and its volume of 0.06 m^3 would fit into the payload compartment of a Perseus B UAV. The optical efficiency of the telescope is 37 percent at 288 nm and 64 percent at 300 nm. Atmospheric measurements with a DIAL laser system have been performed, and the measured ozone density has matched the data from ozonesondes to an altitude of 7 km.

14. SUBJECT TERMS	15. NUMBER OF PAGES
Lidar receiver; DIAL; Ozone	40
	16. PRICE CODE: A03

17. SECURITY CLASSIFICATION OF REPORT	18. SECURITY CLASSIFICATION OF THIS PAGE	19. SECURITY CLASSIFICATION OF ABSTRACT	20. LIMITATION OF ABSTRACT
Unclassified	Unclassified	Unclassified	UL